이학석사 학위논문

A Study of $Mn_xZn_{1-x}Fe_2O_4$ Superparamagnetic Iron Oxide Nanoparticles and its Therapeutic Efficacy for Magnetic Nanoparticle Hyperthermia Applications

초상자성 산화철 나노입자의 개발과
고온열 치료의 유효성 평가

2017년 8월

서울대학교 대학원

의학과 협동과정 종양생물학 전공

이 주 영

A Study of $Mn_xZn_{1-x}Fe_2O_4$ Superparamagnetic Iron Oxide Nanoparticles and its Therapeutic Efficacy for Magnetic Nanoparticle Hyperthermia Applications

August, 2017

Seoul National University

Department of Medicine, Cancer Biology

Jooyoung Lee

초상자성 산화철 나노입자의 개발과 고온열 치료의 유효성 평가

지도 교수 백 선 하

이 논문을 이학석사 학위논문으로 제출함

2017년 8월

서울대학교 대학원
협동과정 종양생물학 전공
이 주 영

이주영의 이학석사 학위논문을 인준함

2017년 8월

위 원 장 박 성 혜 (인)

부위원장 백 선 하 (인)

위 원 강 건 욱 (인)

A Study of $Mn_xZn_{1-x}Fe_2O_4$ Superparamagnetic Iron Oxide Nanoparticles and its Therapeutic Efficacy for Magnetic Nanoparticle Hyperthermia Applications

by Jooyoung Lee

A Thesis Submitted to the Interdisciplinary Graduate Program
in Partial Fulfillment of the Requirements for the
Degree of Master of Philosophy in Cancer Biology
at Seoul National University

August 2017

Approved by Thesis Committee:

Professor Sung Hye Park

Professor Sun Ha Paek

Professor Keon Wook Kang

ABSTRACT

A Study of $Mn_xZn_{1-x}Fe_2O_4$ Superparamagnetic Iron Oxide Nanoparticles and its Therapeutic Efficacy for Magnetic Nanoparticle Hyperthermia Applications

Seoul National University
Department of Medicine, Cancer Biology
Jooyoung Lee

Magnetic nanoparticles are nano-sized (less than 1 micro meter in diameter) material including iron, cobalt, and nickel. The physical & chemical properties, behavior, characteristics of magnetic nanoparticles largely depends on the synthesis method and chemical structure. In this study, we have synthesized iron oxide nanoparticles with controlled doping level of manganese and zinc, and also characterized the magnetic properties of these nanoparticles. We found that $Mn_{0.5}Zn_{0.5}Fe_2O_4$ nanoparticle exhibits highest AC heating characteristics at 30~370 kHz frequency and

80~160 Oe magnetic field strengths. Surface modification of $Mn_{0.5}Zn_{0.5}Fe_2O_4$ were successfully done with methoxy-PEG-silane, confirmed with infrared spectroscopy and dynamic light scattering. Moreover, we investigated the *in vitro* cytotoxic effect and qualitative uptake behavior of superparamagnetic nanoparticle on several kinds of glioblastoma cells. However, to consider the biologically and physiologically safe range of magnetic field, we fixed the frequency with 99.0 kHz and the magnetic field with 140 Oe. *in vivo* magnetic nanoparticle hyperthermia study was done with subcutaneous mouse tumor models, indicating that the magnetic hyperthermia can help to resist the tumor growth and tumor survival. However, magnetic nanoparticle hyperthermia therapy cannot completely cured the tumor, but the hyperthermia treatment inhibited the tumor growth rate.

Keywords: magnetic hyperthermia, superparamagnetic nanoparticle, tumor therapy, intratumoral application

TABLE OF CONTENTS

LIST OF FIGURES

Figure 6. AC magnetic field generation system with optical sensor and PC.

Figure 7. AC magnetically induced self-heating characteristics of $Mn_xZn_{1-x}Fe_2O_4$ solid state nanoparticles.

Figure 8. *in vitro* cytotoxicity (cell viability) assay of PEGylated $Mn_{0.5}Zn_{0.5}Fe_2O_4$ nanoparticles on different kinds of human glioblastoma cells and normal cortex cells.

Figure 9. TEM images of the cells with PEGylated $Mn_{0.5}Zn_{0.5}Fe_2O_4$ nanoparticles.

Figure 10. Thermal image of a mouse tumor model exposed to AC magnetic field for 20 minutes after injection with PEGylated $Mn_{0.5}Zn_{0.5}Fe_2O_4$ nanoparticles.

LIST OF TABLES

LIST OF ABBREVIATIONS AND SYMBOLS

AC, Alternative Current

CCK-8, Cell Counting Kit-8

DMEM, Dulbecco's Modified Eagle's Medium

DC, Direct Current

DLS, Dynamic Light Scattering

EDS, Energy Dispersive X-ray Spectroscopy

FBS, Fetal Bovine Serum

GBL, Glioblastoma

Hc, Coercivity

HTTD, High Temperature Thermal Decomposition

kHz, kilohertz

MNH, Magnetic Nanoparticle Hyperthermia

Ms, Saturation Magnetization

nm, nanometers

NPs, Nanoparticles

NSC, Neuronal Stem Cell

Oe, Oersted

PBS, Phosphate Buffered Saline

PEG, Polyethylene Glycol

PDI, Polydispersity Index

SLP, Specific Loss Power

SPNP, Superparamagnetic Nanoparticle

TEM, Transmission Electron Microscopy

VSM, Vibrating Sample Magnetometer

INTRODUCTION

For several decades, there has been a lot of biomedical applications and preclinical trials using nanoparticles (NPs). [1] The majority of the researchers has been developing and inventing nanostructured materials such as iron oxide nanoparticles (IONPs), gold nanoparticles (GNPs), quantum dots (QDs), carbon nanotubes (CNTs) and these kind of nanostructured materials can be applied for biomedical approaches such as tumor treatment, drug delivery system, biomolecular imaging, and biosensors.

Magnetic nanoparticles are nano-sized (less than 1 micro meter in diameter) material including iron, cobalt, and nickel. The physical & chemical properties, behavior, characteristics of magnetic nanoparticles largely depends on the synthesis method and chemical structure. In most cases, the particle diameter range from 1~100 nm may display

superparamagnetism. [2] When it comes to define that a material is superparamagnetic, it is a type of magnetism that occurs in a small sized ferrimagnetic or ferromagnetic nanoparticles. [3] And also, these kinds of nanoparticles are called as single-domain particles. Moreover, magnetic nanoparticles show a specific preference for the direction, which means the magnetization of nanoparticle is directionally dependent. We call these preferred direction as 'uniaxial anisotropy'. Magnetic nanoparticle that has uniaxial anisotropic characteristic can randomly flip the direction of surrounding magnetization. [4] This effect is caused by thermal energy. The average time to carry out such a flip is given by the relaxation time, τ:

$$\tau = \tau_0 exp\left(\frac{\Delta E}{k_B T}\right) = \tau_0 exp\left(\frac{KV}{k_B T}\right) \quad (1)$$

where τ_0 is the relaxation time constant, k_B Boltzmann constant, T the temperature (k_B multiply by T, $k_B T$ is the thermal energy), ΔE the energy barrier that the amount of magnetization flip has to overcome by thermal energy, K anisotropy constant, and V the volume of single particle.

As described previously, there are so many kinds of approaches for applying nanotechnology and nanoscience on biomedical studies. Among them, the most representative method for treating tumor is magnetic nanoparticle hyperthermia (MNH). Before describing MNH, a word hyperthermia (also called as thermal therapy or thermotherapy) is defined as a type of cancer treatment in which the regional tissue temperature is higher than surrounding body temperature. Hyperthermia treatment can be classified into three subordinate concepts, such as whole body hyperthermia (WH), regional hyperthermia (RH), and local hyperthermia (LH). Whole body hyperthermia is applied for treating metastatic cancer that has been spread throughout the body. This kind of metastatic cancer can be treated by several techniques that can raise the body temperature to 42~43 ℃, with using hot water baths or blankets, or thermal chambers such as large incubator. Regional hyperthermia is a method elevating temperature of large areas such as organs, body cavity, or limb. It includes heating deep seated tumors such as cervical or bladder cancer, or treating

specific organs with using external devices such as radiofrequency energy, microwave, or laser. However, these two kinds of hyperthermia (WH, RH) treatment are usually used with multimodal methods such as chemotherapy or radiation therapy, which can induce the systemic or chemical side effects causing unwanted damage to the surrounding tissues or cells, and injurious physiological response followed by the heat induction of the body under the AC magnetic or electric fields. Lastly, local hyperthermia is one of the concept that can heat a small area of body, such as local tumors. In this kind of hyperthermia, heat can be generated by specific form of delivered energy such as radiofrequency, microwave, ultrasound, laser, and magnetic field. Furthermore, in order to improve the shortcoming of WH and RH, *in vivo* magnetic hyperthermia using magnetic substances such as superparamagnetic nanoparticles, so called as magnetic nanofluid hyperthermia, has been vigorously studied.

Recently, there are a variety of combined therapy using hyperthermia with conventional therapy such as radiation therapy, chemotherapy, etc. Rao et al. previously described hyperthermia combined with radiation therapy and chemotherapy on malignant tumors. [5] They described thermal combination therapy as three different categories: thermal radiotherapy, thermal chemotherapy, and thermal radiochemotherapy. All of these three combined therapy has respective roles for sensitizing malignant tumors.

- Thermal radiosensitization: hyperthermia can directly kill radiation-insensitive S-phase cells and hypoxic cells, also inhibits repair of DNA damage after a sublethal dose of ionizing radiation, which improves the treatment outcome of combination therapy.
- Thermal chemosensitization: hyperthermia can enhance tumor sensitivity to chemotherapeutic drugs, increases the uptake rates of drugs, and also helps drug accumulation in tumor tissues, which can maximize therapeutic outcome of chemotherapy.
- Thermal radiochemosensitization: compared with radiation therapy

alone, radiochemotherapy, and thermoradiotherapy, a form of concurrent chemotherapy and radiation therapy combined with hyperthermia shows the lowest survival rate of tumor cells and has more synergistic effects that can results in beneficial therapeutic outcome.

In addition, a detailed mechanism of hyperthermia-combined therapy can be:

- Inhibition of DNA repair process
- Inhibition of tumor vascular endothelial growth factors
- Cell cycle blockage
- Reduction of interstitial fluid pressure
- Enhanced drug release by changes in cell membrane potential and permeability
- Heat induced apoptosis
- Immune response to hyperthermia
- Increased blood flow and oxygenation after hyperthermia

In this study, we have synthesized iron oxide nanoparticles with controlled doping level of manganese and zinc, and also characterized these magnetic properties of these nanoparticles. We found that $Mn_{0.5}Zn_{0.5}Fe_2O_4$ nanoparticle exhibits highest AC heating characteristics at 30~370 kHz frequency and 80~160 Oe magnetic field strengths. Surface modification of $Mn_{0.5}Zn_{0.5}Fe_2O_4$ were successfully done with methoxy-PEG-silane, confirmed with infrared spectroscopy and dynamic light scattering. Moreover, we investigated the cytotoxic effect and qualitative uptake behavior of superparamagnetic nanofluid on several kinds of glioblastoma cells, evaluated magnetic nanofluid hyperthermia effect on mouse tumor models.

MATERIALS AND METHODS

I. Preparation of Superparamagnetic Iron Oxide Nanoparticles

Reagents and chemicals

Fe (III) acetylacetonate (> 99.9 %, precursor), Mn (II) acetate tetrahydrate (99.99 %, precursor), Zn (II) acetate dihydrate (99.999 %, precursor), oleic acid (90 %, surfactant), oleylamine (70 %, surfactant), and benzyl ether (99 %, solvent) were purchased from Sigma-Aldrich Chemical Co., and 1,2-hexadecanediol (> 98 %, reductant) were purchased from Tokyo Chemical Industries Co. Table 1 shows the name, chemical & linear formula, molecular weight, and purity of compounds used for the synthesis of superparamagnetic $Mn_xZn_{1-x}Fe_2O_4$ nanoparticles.

Synthesis of solid-state $Mn_xZn_{1-x}Fe_2O_4$ nanoparticles

For the synthesis of solid state $Mn_xZn_{1-x}Fe_2O_4$ nanoparticles, 2 mmol of iron acetylacetonate (precursor), 0.1~0.9 mmol of Mn acetate tetrahydrate & Zn acetate dihydrate, 10 mmol of 1,2-hexadecanediol (reductant), 6 mmol of oleic acid & oleylamine (surfactant), and 20mL of benzyl ether (solvent) were mixed and magnetically stirred in three neck round bottom flask.

Magnetic nanoparticles are synthesized with in-house method, which is first reported in 2011 [13]. In conventional high temperature thermal decomposition (HTTD) method, the mixed chemicals were heated up to ~200 ℃ for 30 minutes (~6 ℃/minute) and maintained another 30 minutes as nucleation step, and then heated again to 296 ℃ (boiling point of benzyl ether) for 6~8 minutes (14~16 ℃/minute) and maintained 30 minutes as growth step. However, when it comes to the modified HTTD method, the heat elevation time in the nucleation step were changed to 20

minutes (~10 ℃/minute), and maintained another 60 minute. The maintaining time in the growth step were changed to 47 minutes to control the average diameter of synthesized nanoparticles with below 10 nm. At the end of the sequence, the mixed chemicals were cooled down to 25 ℃ (room temperature), and 40 mL of ethanol was added to the solutions and vigorously stirred for precipitation. Synthesized nanoparticles were rinsed with sonication, precipitated and separated with a centrifuge. The products were then dispersed in 15 mL of hexane and 30 mL of ethanol and sonicated with ultrasonic cleanser for 10 minutes to remove organic residues. After centrifugation with 6500 rpm for 10 minutes, the nanoparticles were collected and dried at vacuum oven. Figure 1~3 shows the procedure of HTTD method.

Surface modification of synthesized nanoparticles

The synthesized nanoparticles were coated with biocompatible polymer, methoxy-PEG-silane with 500 Daltons. For coating of the PEG layer, the

surface of synthesized nanoparticles was first modified by oleic acid. 3 mL of oleic acid and 0.7 mL of ammonium chloride were added in the solution of ethanol with nanoparticles. The mixture was vigorously agitated for 2 hours, then washed with acetone after the nanoparticles were precipitated by permanent magnet to give oleic acid coated nanoparticles. The oleic acid modified nanoparticles was dispersed in 7.5 mL of toluene and then 3.75 mL of triethylamine and 0.75 mL of methoxy-PEG-silane 500 Dalton were added. The mixed solution were agitated well for 24 hours. The PEGylated nanoparticles in the solution were washed with pentane and dispersed in deionized water to form nanofluidic solutions.

II. Material Characterization

Vibrating Sample Magnetometer

The magnetic properties such as coercivity (Hc) at minor hysteresis loops, saturation magnetization (Ms) at major hysteresis loops, and initial magnetization curves of superparamagnetic nanoparticles were investigated by using vibrating sample magnetometer (VSM). In this study, measurement of the magnetic properties of the synthesized $Mn_xZn_{1-x}Fe_2O_4$ nanoparticles were performed by placing 15~20 mg of solid state nanoparticles in a VSM holder at room temperature. The applied magnetic fields were ± 150 Oe for minor hysteresis loop, and ± 15 kOe for major hysteresis loop.

Dynamic Light Scattering

The size, size distribution, zeta potential, and polydispersity index (PDI) of the PEGylated nanoparticles were measured by using a dynamic light

scattering (DLS), to investigate the dispersion status, aggregation (PDI), and surface charge of the PEGylated nanoparticles (z-potential), which affect the magnetic reactivity, AC magnetically induced heating effects, and also the cellular uptake efficiency.

Measurement of AC magnetically generated heating characteristics

The AC magnetically induced heating temperatures of solid state and PEGylated nanoparticles were measured by using specially designed device named HF induction generator, which can generate magnetic fields, consists of AC coils, water chiller, capacitors, DC power supplies, function generators, optical thermometers, and a PC system as shown in figure 6. The AC magnetic field generation system operates at a range of 30~370 kHz frequencies, magnetic field strengths with 80~160 Oe with no change of the AC coil or capacitor. This is instrumental because it is able to evaluate the AC heating behavior of various nanoparticles over a wide range of frequencies and magnetic field strengths because nanoparticles

show the different AC heating characteristics, which is depending on magnetism of the material, the given frequency and magnetic field strengths. The total amount of solid state nanoparticles for measuring the AC self-heating effects were fixed at 60 milligrams. In order to experimentally calculate the SLP value, the PEGylated nanoparticles were dispersed in various kinds of fluids with various concentrations, and the AC self-heating effects of the fluids containing PEGylated nanoparticles was measured under the applied AC magnetic field.

III. *in vitro* & *in vivo* Assessments

Ethics statement

Fresh human tissue samples were obtained with the required Institutional Review Board (IRB) approval from Seoul National University Hospital (IRB No. H-0507-509-153).

Cell culture

Seven types of glioblastoma cell lines (A172, T98G, U118, U138, U251, U373, and U87), two types of primary glioblastoma cells (GBL-28 and GBL-37) are used for this study. Commercially available human glioblastoma cell lines are obtained from the American Type Culture Collection (ATCC; Manassas, VA, USA) and Korean Cell Line Bank (KCLB: Seoul, Korea). GBL-28 and GBL-37 are obtained from brain tumor lobectomy. Brain tumor is diagnosed as glioblastoma after pathological analysis. The tumor mass were cultured in the laboratory, and the obtained

glioblastoma cells were used for the further study. For the comparison study, human brain normal cortex cells (NSC09, NSC10) were used. All of the cells are cultured with using Dulbecco's Modified Eagle's Medium (DMEM), containing 10 % fetal bovine serum (FBS) and 1 % antibiotic-antimycotic (AA) in a humidified incubator with 5 % CO_2 at 37 ℃.

in vitro cytotoxicity assay

For *in vitro* cytotoxicity assay, CCK-8 assay was conducted to evaluate the effects of PEGylated $Mn_{0.5}Zn_{0.5}Fe_2O_4$ nanoparticles for proliferation and viability. CCK-8 assay were used by following manufacturer instructions. A172, T98G, U118, U138, U251, U373, U87, GBL-28, GBL-37, NSC09, NSC10 cells are seeded with the number of 3000 cells/well in 96 well plate. After 24 hours (inoculation time), PEGylated $Mn_{0.5}Zn_{0.5}Fe_2O_4$ nanoparticles are treated at the concentrations of 0, 3, 5, 10, 30, 50, 100, 300, and 500 μg/mL for 24 hours in an incubator at 5 % CO_2, 37 ℃ humidified incubator. After incubation with PEGylated $Mn_{0.5}Zn_{0.5}Fe_2O_4$ nanoparticles, each well

were washed with phosphate buffered saline, and fresh media with CCK-8 solution were pipetted to each well of the 96 well plate. The plate were incubated another 2 hours, for the reaction of CCK-8 solution and the cells. Finally, the absorbance at 450 nm wavelength is evaluated using a Multiscan MS spectrophotometer.

Cellular uptake of PEGylated $Mn_{0.5}Zn_{0.5}Fe_2O_4$ nanoparticles

TEM analysis for the cells treated by the PEGylated $Mn_{0.5}Zn_{0.5}Fe_2O_4$ nanoparticles were conducted to investigate the quantitative nanoparticle's internalization into the cells, localization of the nanoparticles, and the morphological analysis of the cells. Experiments were done at the department of research & experiment, biomedical research institute, Seoul national university hospital. In brief, the cells were incubated with 100 μg/mL nanoparticle for 24 hours. After incubation, cells were washed and detached with TrypLE solution, and subsequently fixed overnight in several kinds of fixation solution. The samples were then embedded epoxy

resin, and appropriate areas for thin sectioning were cut at 65 nm and stained with 6 % uranyl acetate and 4 % lead citrate before examination with a transmission electron microscope (JEM-1400; Japan) at 80 kV.

Animals

in vivo experiments for magnetic nanoparticle hyperthermia were performed on adult male balb/c nude mouse weighing between 20~22 g were housed in the same animal care facility under 12 hours light/dark cycle with food and water provided. All efforts were conducted to minimize suffering and number of animals used in this experiments.

Mouse tumor models

Animal care and subcutaneous murine fibrosarcoma (FSaLL) cell injection, and *in vivo* hyperthermia experiment were conducted in accordance with guidelines approved by the Institutional Animal Care and Use Committee (IACUC) of Seoul National University (IACUC No. SNU-161129-2). All

of the procedures were done by reducing the amount of pain caused to the Balb/c nude mouse. For subcutaneous mouse tumor models, Mouse used in this experiment were anesthetized and FSaLL cells ($5x10^6$ cells with volume of 50 μL) were administered by subcutaneous injection into the proximal thigh region of Balb/c nude mouse.

in vivo magnetic nanoparticle hyperthermia

Mouse with subcutaneous FSaLL injection were randomly divided into 4 groups (n=5, control group; n=5, nanoparticle treatment without alternating magnetic field; n=5, alternating magnetic field treatment without nanoparticle; n=5, nanoparticle treatment with alternating magnetic field so called as hyperthermia group) and the health condition of the mouse were checked daily. *in vivo* hyperthermia study were started after 10 days of the FSaLL cell injection. Solid-tumor induced mouse models were anesthetized and 100 μL of PEGylated $Mn_{0.5}Zn_{0.5}Fe_2O_4$ nanoparticles were injected at the center of induced tumors. The mouse were placed in the

center of AC coil system for magnetic hyperthermia. Applied magnetic field strength and frequency were 140 Oe and 99.0 kHz (140 Oe equals 11.14 kA/m and the total amount of given magnetic field was 1.103×10^9 A/m•s). For hyperthermia treatment, AC magnetic field were applied for 20 minutes, for 6 times of hyperthermia treatment in 2 weeks. Mouse tumor size and body weight were checked in every 2 days. The volumetric measurement of xenografted tumors were measured by Vernier caliper, and the equation is:

$$\text{Tumor volume } (\text{mm}^3) = \frac{1}{2}(\text{length} \times \text{width}^2) \quad [11]$$

Statistical analysis

All data are expressed as means of ± standard deviation (SD). Statistical significance is determined using a student's t-test. P value under 0.05 is considered statistically significant.

RESULTS AND DISCUSSION

Synthesis of superparamagnetic $Mn_xZn_{1-x}Fe_2O_4$ nanoparticles

The superparamagnetic $Mn_xZn_{1-x}Fe_2O_4$ nanoparticles used in this study were synthesized by modified HTTD method in which the chemical potential of cations were changed by controlling the temperature during the synthesis procedure. This synthesis method includes the decomposition of metallic precursors (iron acetylacetonate) with hot organic surfactants (oleic acid & oleylamine) and solvents (benzyl ether), as shown in figure 1. The basic mechanism of this synthesis method is to initiate chemical reactions between the reagents in solvent and regulate the nucleation and growth step for the synthesis of superparamagnetic $Mn_xZn_{1-x}Fe_2O_4$ nanoparticles by changing the reaction temperature of the solution. The HTTD method offers significant advantages, such as controlling the size and the size distribution of synthesized nanoparticles, helps to generate powerful AC heating characteristics of the nanoparticles, which also

explained as enhanced magnetic properties, and lastly this method can be easily called up for massive production. [6] After the synthesis of $Mn_xZn_{1-x}Fe_2O_4$, the total amount of obtained solid state nanoparticles were approximately 130~150 milligrams in average. For prevention of chemical change or the damping, the synthesized nanoparticles are stored at the air-tightened vacuum desiccator.

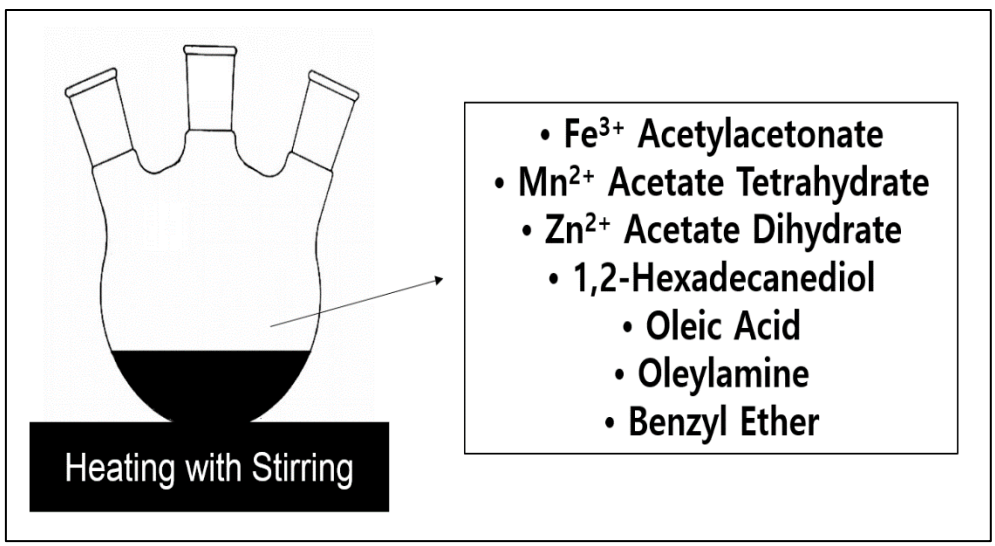

Figure 1. Schematic diagram & reagents for the synthesis of superparamagnetic $Mn_xZn_{1-x}Fe_2O_4$ nanoparticles.

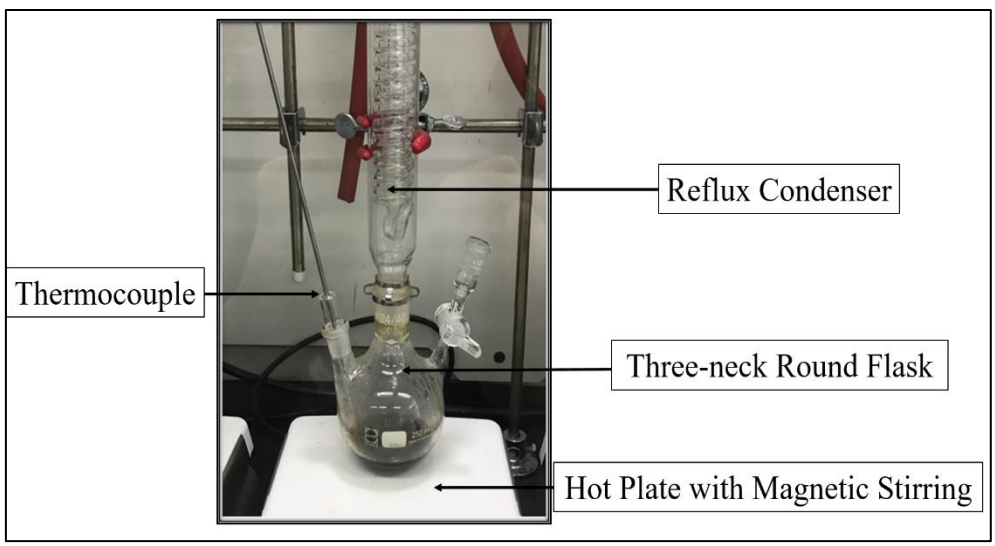

Figure 2. A picture of synthesis procedure including thermocouple, reflux condenser, three-neck round flask, hot plate, and magnetic stirring.

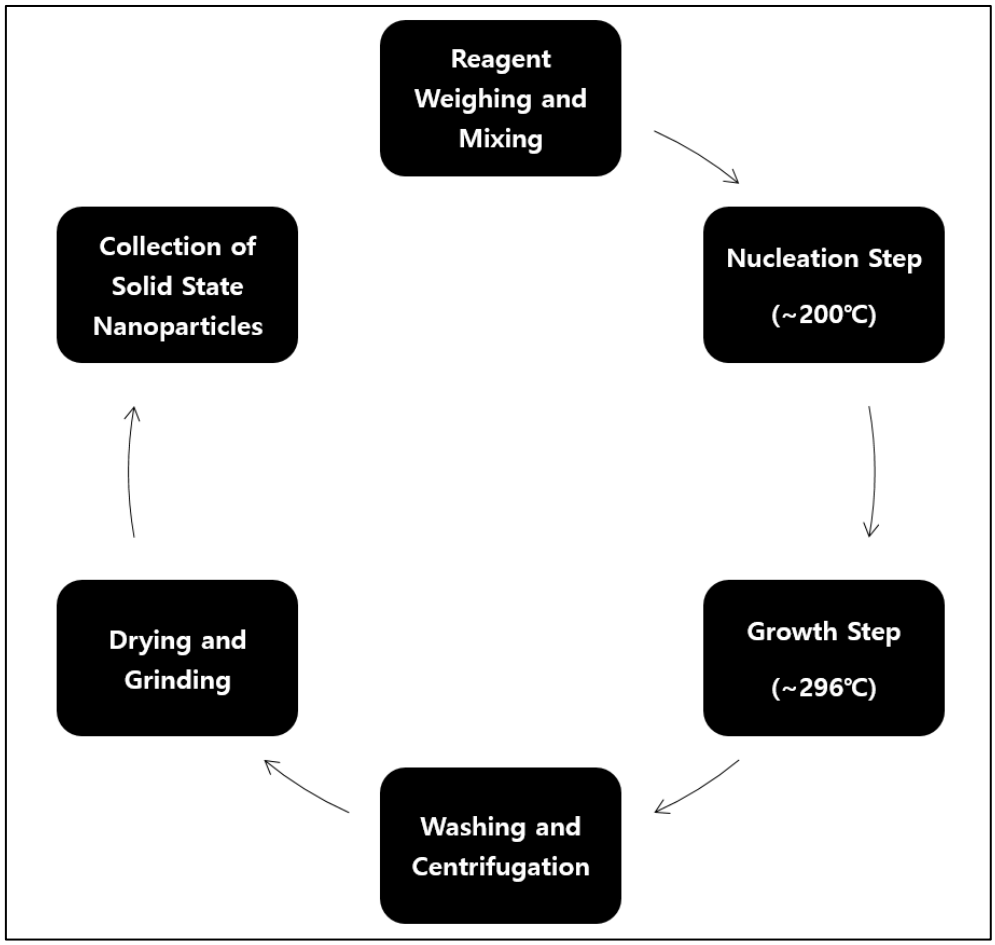

Figure 3. Six-step sequential procedure for the synthesis of superparamagnetic $Mn_xZn_{1-x}Fe_2O_4$ nanoparticles.

Name of Compound	Chemical Formula	Linear Formula	Molecular Weight	Purity
Iron (III) acetylacetonate	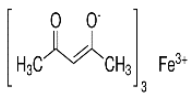	$Fe(C_5H_7O_2)_3$	353.17	≥99.9 %
Mn (II) acetate tetrahydrate	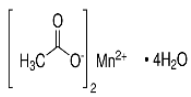	$(CH_3COO)_2Mn•4H_2O$	245.09	99.99 %
Zn (II) acetate dihydrate	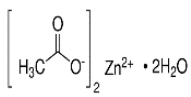	$Zn(CH_3COO)_2•2H_2O$	219.51	99.999%
1,2-Hexadecanediol	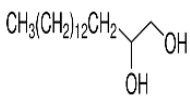	$CH_3(CH_2)_{13}CHOHCH_2OH$	258.44	≥98.0 %
Oleic Acid	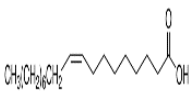	$CH_3(CH_2)_7CH=CH(CH_2)_7$ COOH	282.46	90 %
Oleylamine	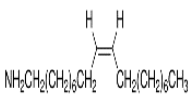	$CH_3(CH_2)_7CH=CH(CH_2)_7$ CH_2NH_2	267.49	70 %
Benzyl Ether	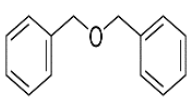	$(C_6H_5CH_2)_2O$	198.26	98 %

Table 1. Name, chemical & linear formula, molecular weight, and purity of compounds used for the synthesis of superparamagnetic $Mn_xZn_{1-x}Fe_2O_4$ nanoparticles.

	Fe^{3+}	Mn^{2+}	Zn^{2+}	HDD	O.A.	O.M.	B.E.
X=0	2 mmol	-	1.0 mmol	10 mmol	6 mmol	6 mmol	20 mL
X=0.1		0.1 mmol	0.9 mmol				
X=0.2		0.2 mmol	0.8 mmol				
X=0.3		0.3 mmol	0.7 mmol				
X=0.4		0.4 mmol	0.6 mmol				
X=0.5		0.5 mmol	0.5 mmol				
X=0.6		0.6 mmol	0.4 mmol				
X=0.7		0.7 mmol	0.3 mmol				
X=0.8		0.8 mmol	0.2 mmol				
X=0.9		0.9 mmol	0.1 mmol				
X=1		1.0 mmol	-				

Table 2. Total amount of reagents mixed for synthesis of superparamagnetic $Mn_xZn_{1-x}Fe_2O_4$ nanoparticles.

Characterization of synthesized $Mn_xZn_{1-x}Fe_2O_4$ nanoparticles

To investigate that the synthesized nanoparticles are superparamagnetic, each of $Mn_xZn_{1-x}Fe_2O_4$ nanoparticles were analyzed with TEM. 11 kinds of synthesized $Mn_xZn_{1-x}Fe_2O_4$ nanoparticles (X=0~1) were measured with TEM, the average diameter of each $Mn_xZn_{1-x}Fe_2O_4$ nanoparticles were below 10 nanometers shown in figure 4-13 and table 4. Each of the diameter were counted 100 times on the image of X 100,000 magnification. In addition, to confirm the doping level of the manganese and zinc, each of the synthesized $Mn_xZn_{1-x}Fe_2O_4$ nanoparticles were analyzed with EDS as shown in figure 4-12 and table 3. Each of the sample analyzed with EDS were measured at the three different sites on the X 50,000 magnification in normal TEM mode, and the detected atomic weight percent of manganese and zinc verified that the dopant were successfully doped depending on the amount of reagent mixed during the synthesis procedure. Finally, the magnetic properties such as coercivity (Hc) in minor magnetic hysteresis loops, saturation magnetization (Ms) in major magnetic hysteresis loops,

initial magnetization slope were measured with VSM, indicating that all of synthesized $Mn_xZn_{1-x}Fe_2O_4$ nanoparticles exhibits the superparamagnetic characteristics.

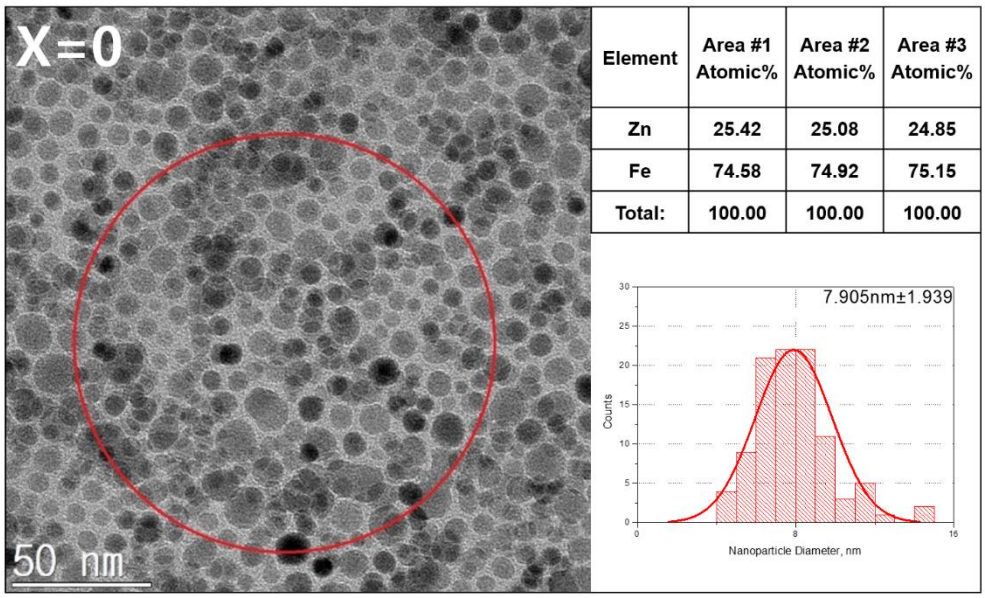

Figure 4-1. TEM and EDS result of synthesized $ZnFe_2O_4$ (X=0)

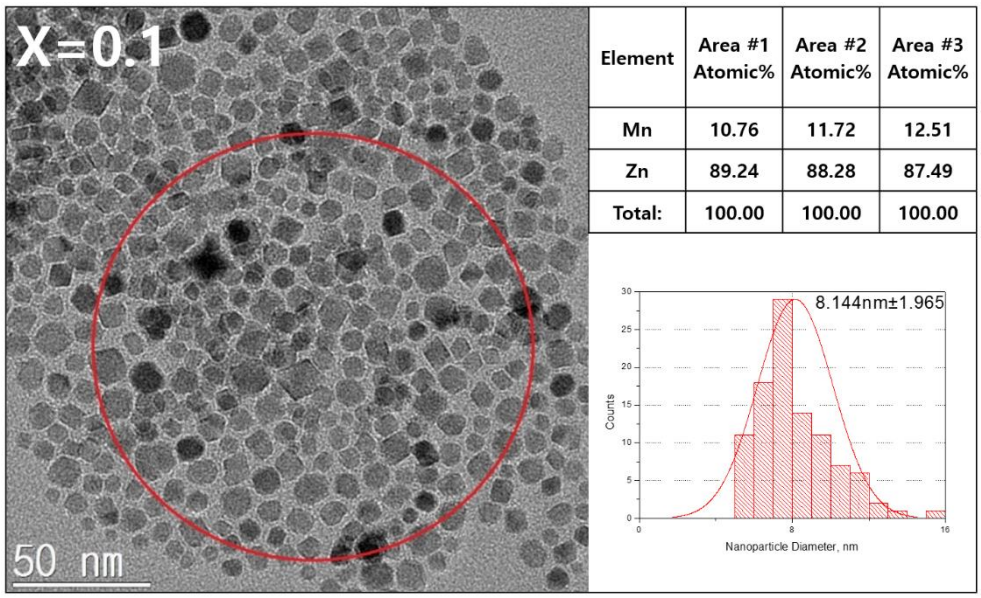

Figure 4-2. TEM and EDS result of synthesized $Mn_{0.1}Zn_{0.9}Fe_2O_4$ (X=0.1)

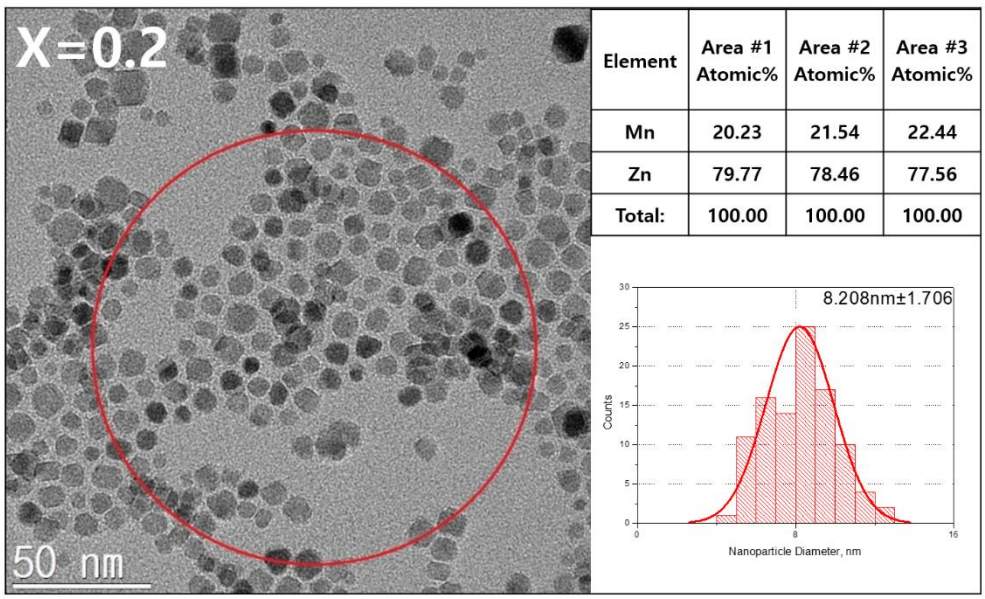

Figure 4-3. TEM and EDS result of synthesized $Mn_{0.2}Zn_{0.8}Fe_2O_4$ (X=0.2)

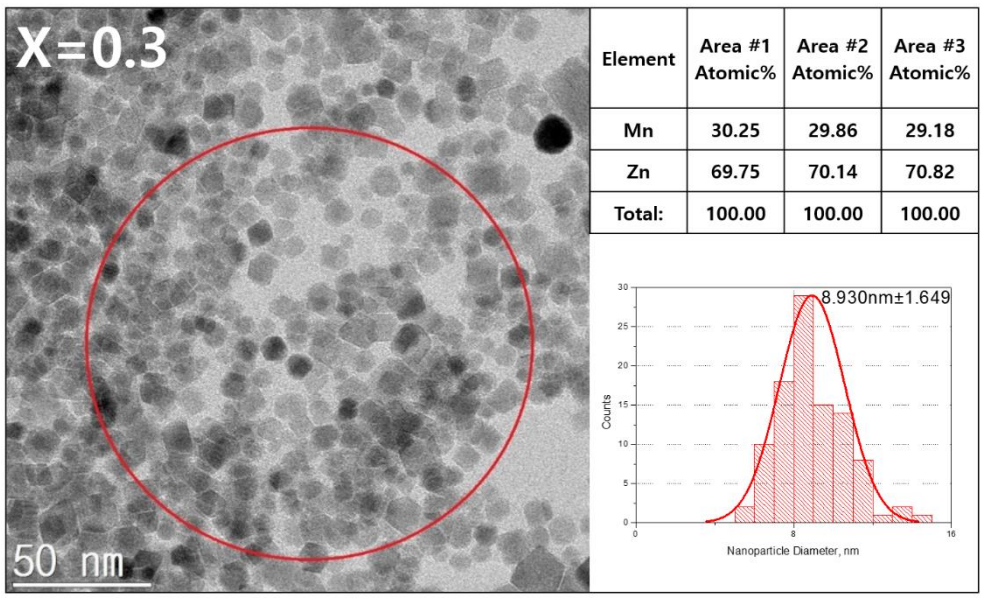

Figure 4-4. TEM and EDS result of synthesized $Mn_{0.3}Zn_{0.7}Fe_2O_4$ (X=0.3)

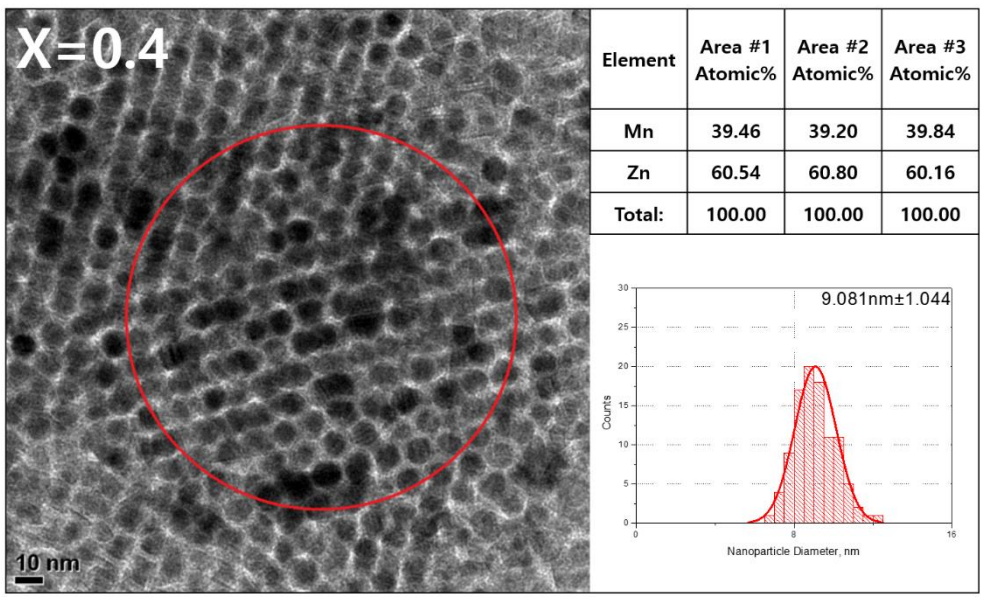

Figure 4-5. TEM and EDS result of synthesized $Mn_{0.4}Zn_{0.6}Fe_2O_4$ (X=0.4)

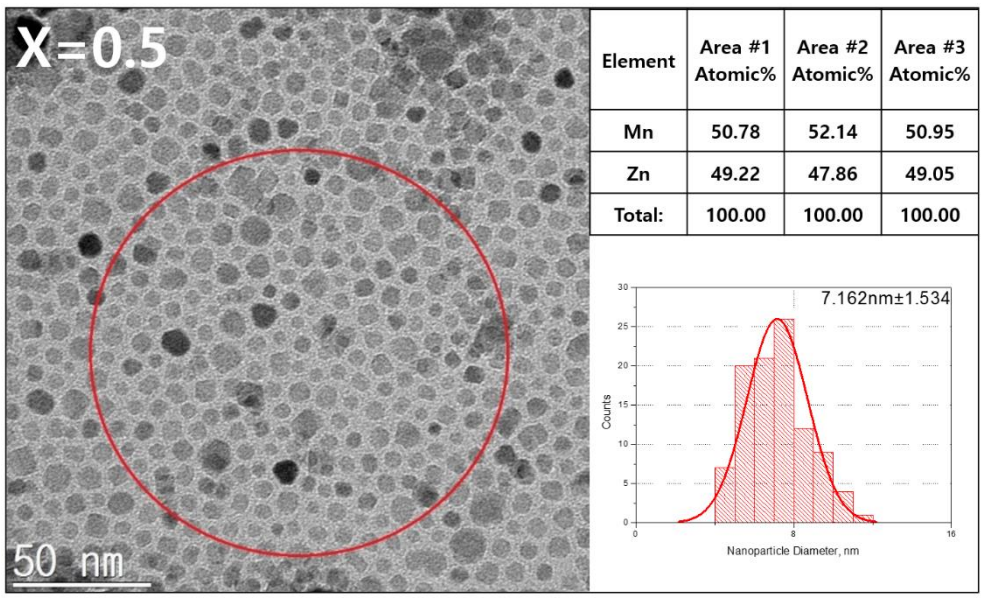

Figure 4-6. TEM and EDS result of synthesized $Mn_{0.5}Zn_{0.5}Fe_2O_4$ (X=0.5)

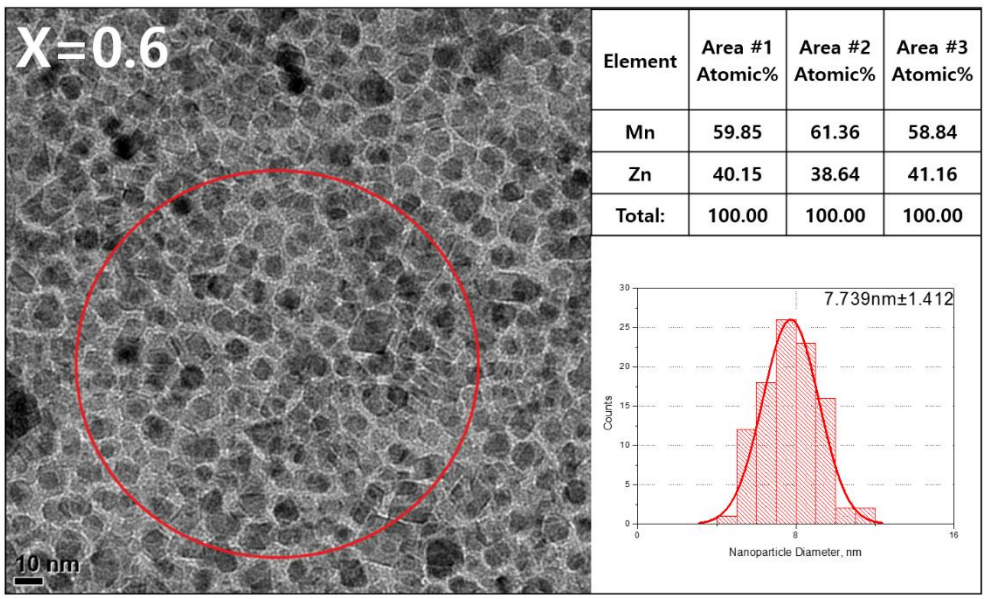

Figure 4-7. TEM and EDS result of synthesized $Mn_{0.6}Zn_{0.4}Fe_2O_4$ (X=0.6)

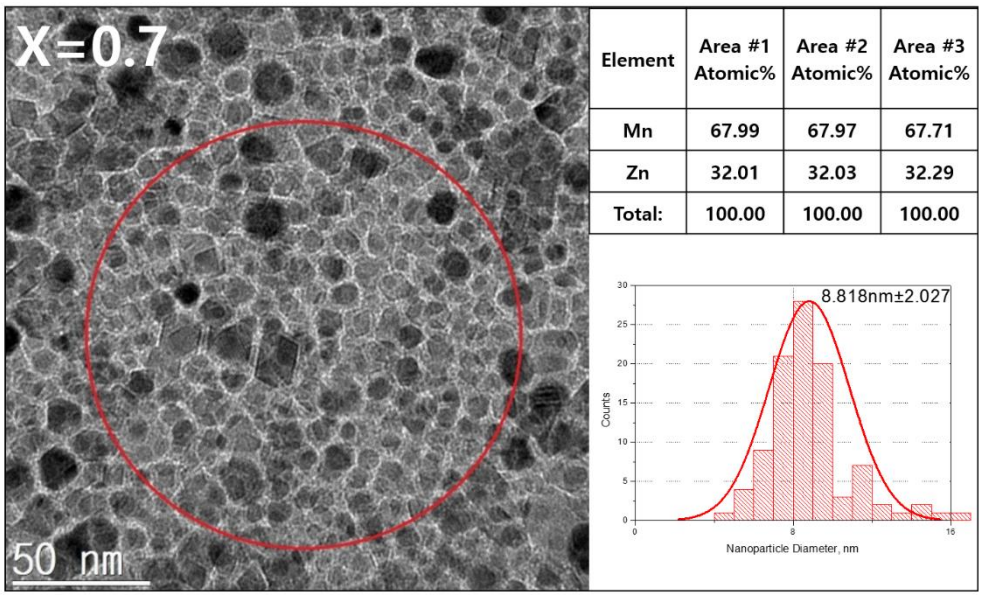

Figure 4-8. TEM and EDS result of synthesized $Mn_{0.7}Zn_{0.3}Fe_2O_4$ (X=0.7)

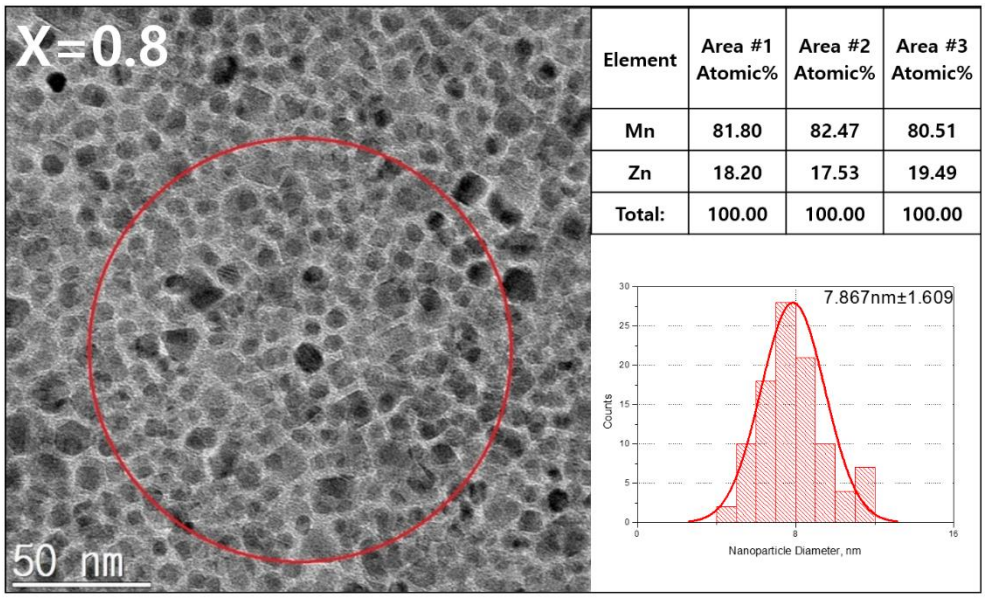

Figure 4-9. TEM and EDS result of synthesized $Mn_{0.8}Zn_{0.2}Fe_2O_4$ (X=0.8)

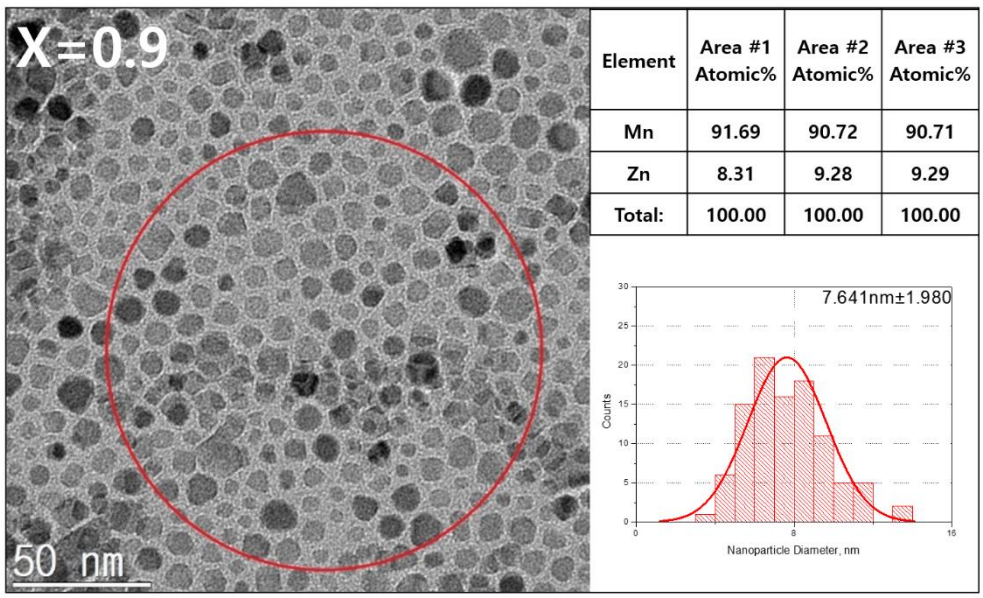

Figure 4-10. TEM and EDS result of synthesized $Mn_{0.9}Zn_{0.1}Fe_2O_4$ (X=0.9)

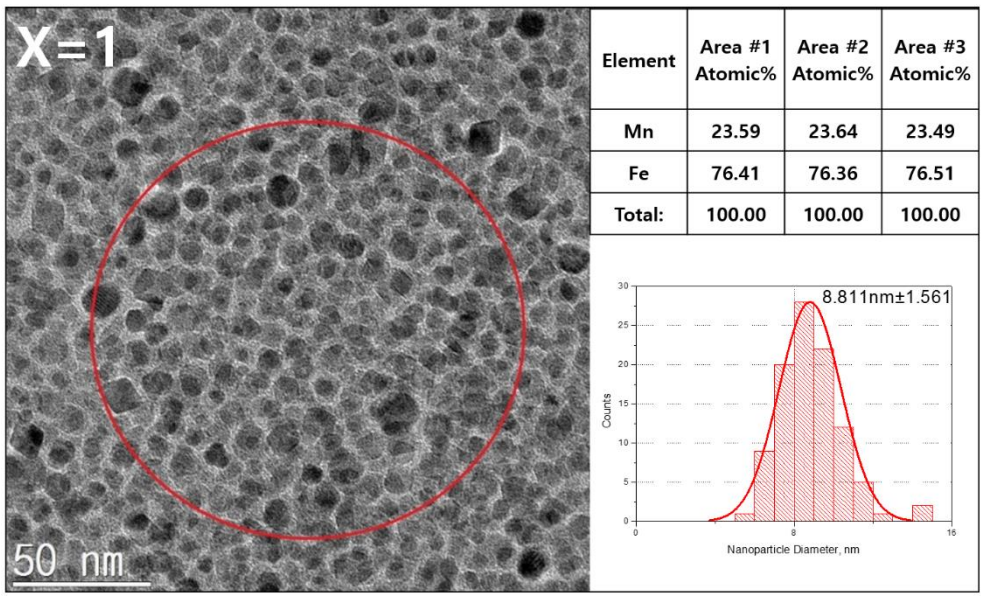

Figure 4-11. TEM and EDS result of synthesized $MnFe_2O_4$ (X=1)

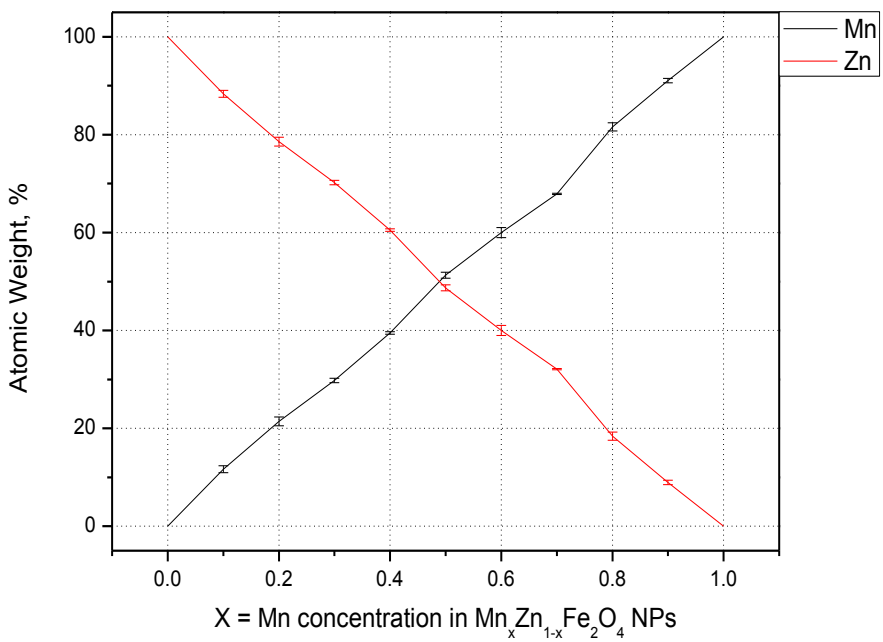

Figure 4-12. Atomic weight percent of detected manganese and zinc after synthesis of $Mn_xZn_{1-x}Fe_2O_4$ nanoparticles.

	Mn	Zn	Fe	Mn (w/o Fe)	Zn (w/o Fe)
X=0	0 %	25.99 %	74.01 %	0 %	100%
X=0.1	2.01 %	16.94 %	81.05 %	11.66 %	88.34 %
X=0.2	3.33 %	13.21 %	83.46 %	21.40 %	78.60 %
X=0.3	4.77 %	11.98 %	83.25 %	29.76 %	70.24 %
X=0.4	5.65 %	9.34 %	84.99 %	39.50 %	60.50 %
X=0.5	7.74 %	7.83 %	84.43 %	51.29 %	48.71 %
X=0.6	9.18 %	6.53 %	84.29 %	60.02 %	39.98 %
X=0.7	11.23 %	5.56 %	83.21 %	67.89 %	32.11 %
X=0.8	14.05 %	3.29 %	82.66 %	81.59 %	18.41 %
X=0.9	16.12 %	1.65 %	82.23 %	91.04 %	8.96 %
X=1	23.57 %	0 %	76.43 %	100%	0 %

Table 3. EDS result (atomic weight percent) of detected manganese and zinc after synthesis of $Mn_xZn_{1-x}Fe_2O_4$ nanoparticles. (w/o Fe: detected proportion of manganese and zinc after calibrated without iron)

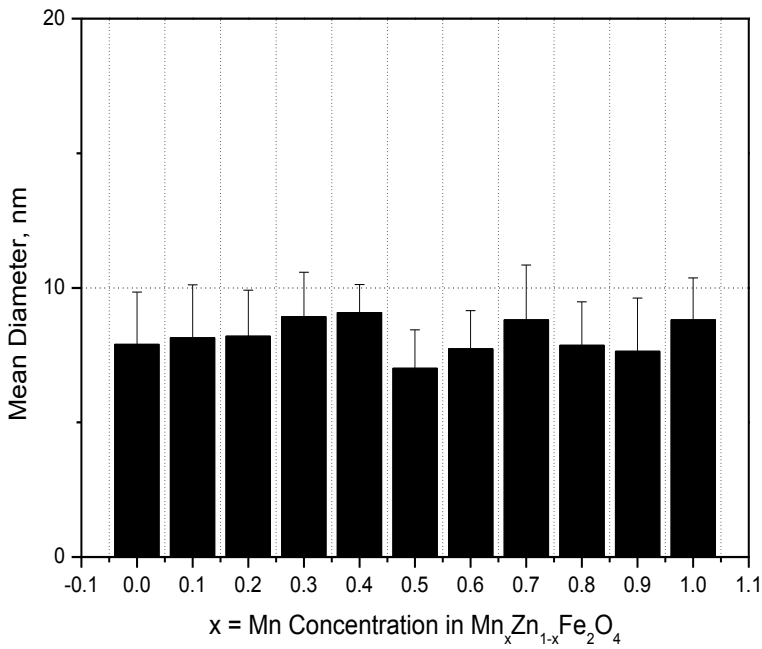

Figure 4-13. Average diameter of synthesized $Mn_xZn_{1-x}Fe_2O_4$ nanoparticles.

Sample	Mean Diameter	Standard Deviation	Counted
X=0	7.905 nm	1.939	100 times
X=0.1	8.144 nm	1.965	100 times
X=0.2	8.208 nm	1.706	100 times
X=0.3	8.930 nm	1.649	100 times
X=0.4	9.081 nm	1.044	100 times
X=0.5	7.008 nm	1.434	100 times
X=0.6	7.739 nm	1.412	100 times
X=0.7	8.818 nm	2.027	100 times
X=0.8	7.867 nm	1.609	100 times
X=0.9	7.641 nm	1.980	100 times
X=1	8.811 nm	1.561	100 times

Table 4. Average diameter of synthesized $Mn_xZn_{1-x}Fe_2O_4$ nanoparticles.

Sample	Coercivity (±150Oe)
X=0	0.72185 G
X=0.1	0.22641 G
X=0.2	2.3662 G
X=0.3	0.56479 G
X=0.4	4.3827 G
X=0.5	6.2855 G
X=0.6	3.2214 G
X=0.7	0.61964 G
X=0.8	0.94044 G
X=0.9	1.3962 G
X=1	1.0420 G

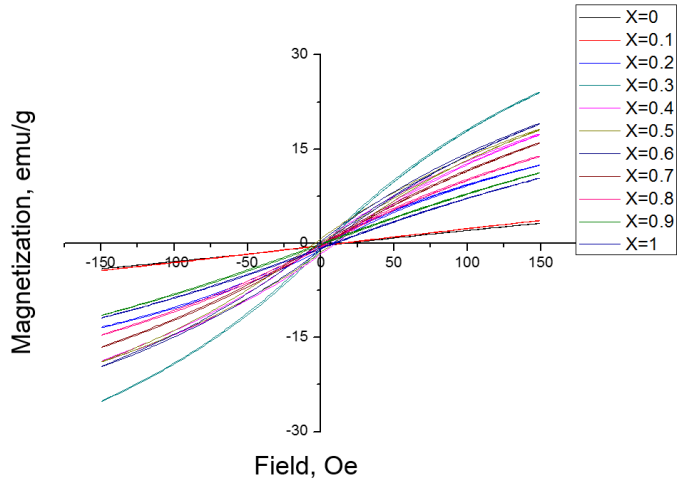

Figure 5-1. VSM measurement of synthesized $Mn_xZn_{1-x}Fe_2O_4$ nanoparticles. (Measured coercivity (Hc) value at ±150 Oe)

Sample	Saturation Magnetization (±15kOe)
X=0	33.054 emu/g
X=0.1	40.038 emu/g
X=0.2	41.048 emu/g
X=0.3	69.808 emu/g
X=0.4	65.675 emu/g
X=0.5	69.744 emu/g
X=0.6	65.694 emu/g
X=0.7	62.771 emu/g
X=0.8	55.688 emu/g
X=0.9	56.033 emu/g
X=1	51.445 emu/g

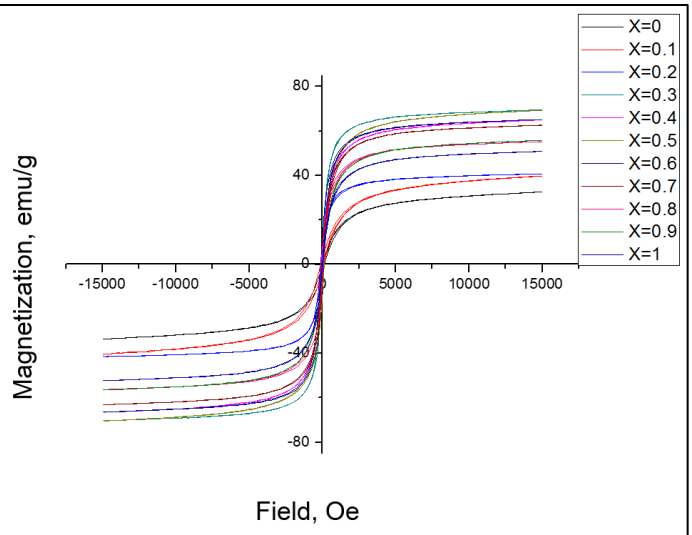

Figure 5-2. VSM measurement of synthesized $Mn_xZn_{1-x}Fe_2O_4$ nanoparticles. (Measured saturation magnetization (Ms) value at ±15 kOe)

Measurement of AC magnetically induced heating characteristics

The AC magnetically induced heating characteristics of solid state $Mn_xZn_{1-x}Fe_2O_4$ nanoparticles and fluid state PEGylated nanoparticles were measured by using specially designed device named HF induction generator, which can generate magnetic fields, consists of AC coils, water chiller, capacitors, DC power supplies, function generators, optical thermometers, and a PC system as shown in figure 6. This device operates at a range of frequencies with 30~370 kHz, with a range of magnetic field strength with 80~160 Oe without changing the AC coil or the capacitor. This is significant because investigating the behavior of the nanoparticles under different frequencies and magnetic field strengths gives us to understand underlying mechanism of the AC self-heating characteristics of the superparamagnetic nanoparticles, because the nanoparticles have different AC self-heating characteristics, which is depending on magnetism of the material, the given frequency and magnetic field strengths.

Figure 6. AC magnetic field generation system with optical sensor and PC.

The total amount of solid state nanoparticle measured for AC heating characteristics were fixed at 60 mg in an Eppendorf-tube. To design the measurement environment as an isolated system (to avoid the interference of AC heating measurement from surrounding atmosphere), each of the samples were located in an insulated Styrofoam at the center of the sample bed. The tip of optical fiber were located at the inside of the Eppendorf-tube containing solid state $Mn_xZn_{1-x}Fe_2O_4$ nanoparticles. 11 kinds of $Mn_xZn_{1-x}Fe_2O_4$ nanoparticles were investigated under 8 different frequencies (31.9, 47.0, 98.9, 140.0, 168.1, 195.5, 239.9, 360.2 kHz) and 5 different magnetic field strengths (80, 100, 120, 140, 160 Oe) as shown in figure 7-1~10. The total magnetic field generation time was 600 seconds in each measurement. When the magnetic field turned on, the AC heating temperature were measured by the optical thermometer, and also cooled down when the magnetic field turned off.

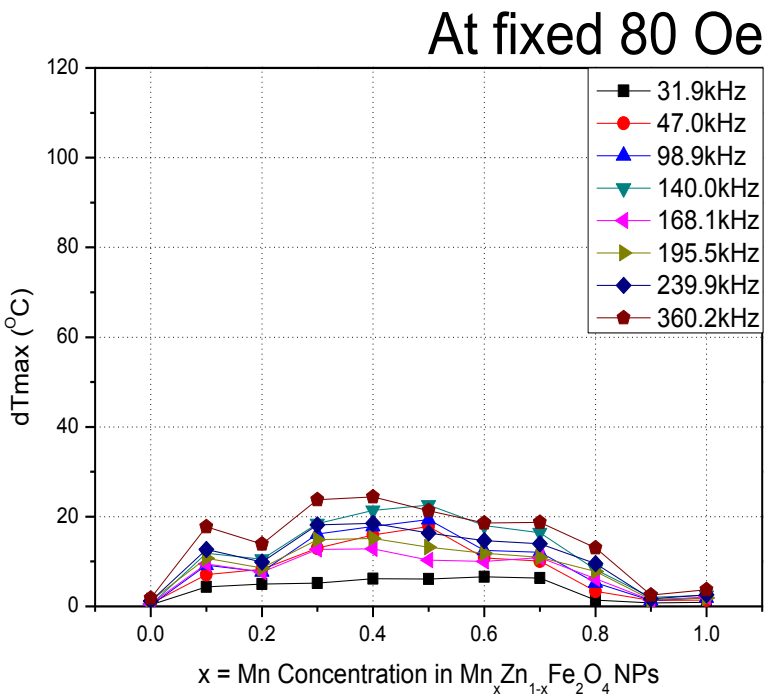

Figure 7-1. AC magnetically induced self-heating characteristics of $Mn_xZn_{1-x}Fe_2O_4$ solid state nanoparticles depending on the Mn concentration at fixed 80 Oe. (t=600 seconds)

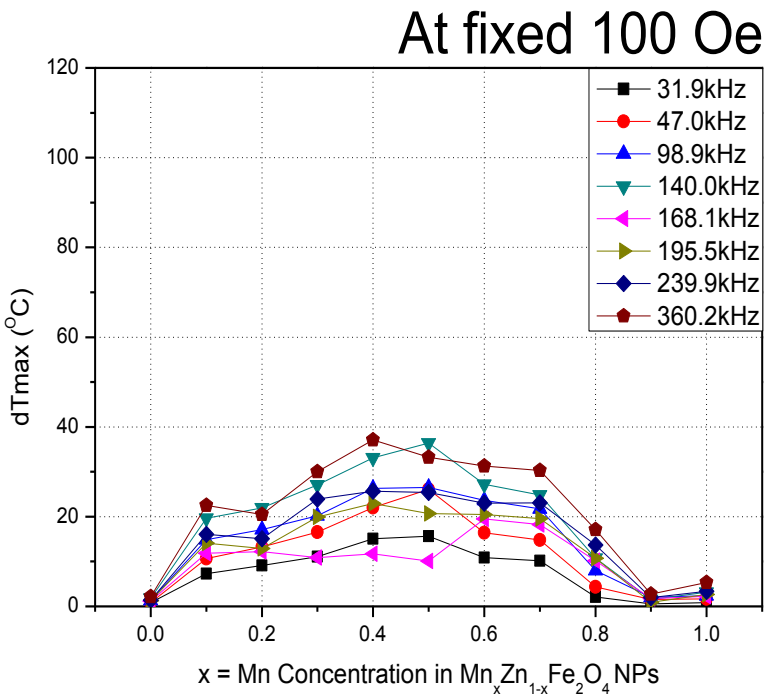

Figure 7-2. AC magnetically induced self-heating characteristics of $Mn_xZn_{1-x}Fe_2O_4$ solid state nanoparticles depending on the Mn concentration at fixed 100 Oe. (t=600 seconds)

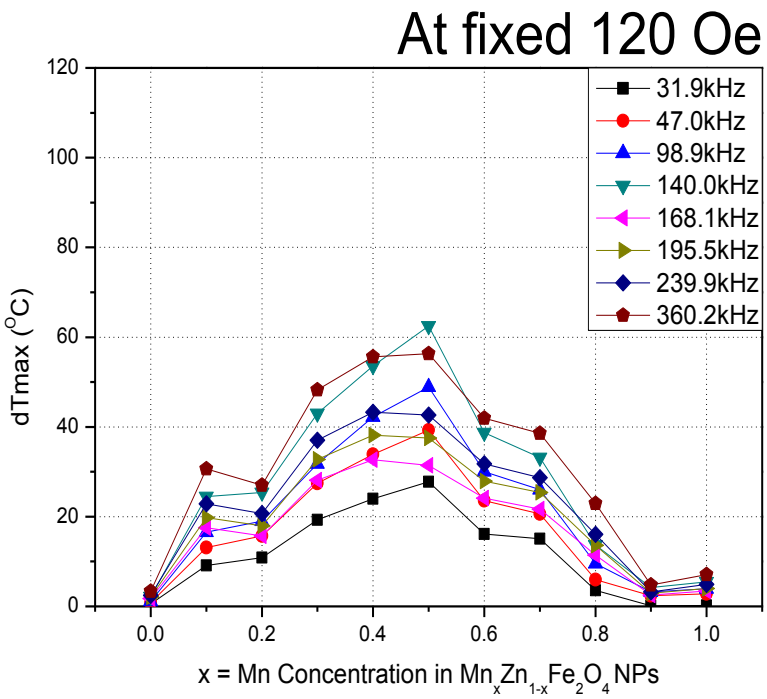

Figure 7-3. AC magnetically induced self-heating characteristics of $Mn_xZn_{1-x}Fe_2O_4$ solid state nanoparticles depending on the Mn concentration at fixed 120 Oe. (t=600 seconds)

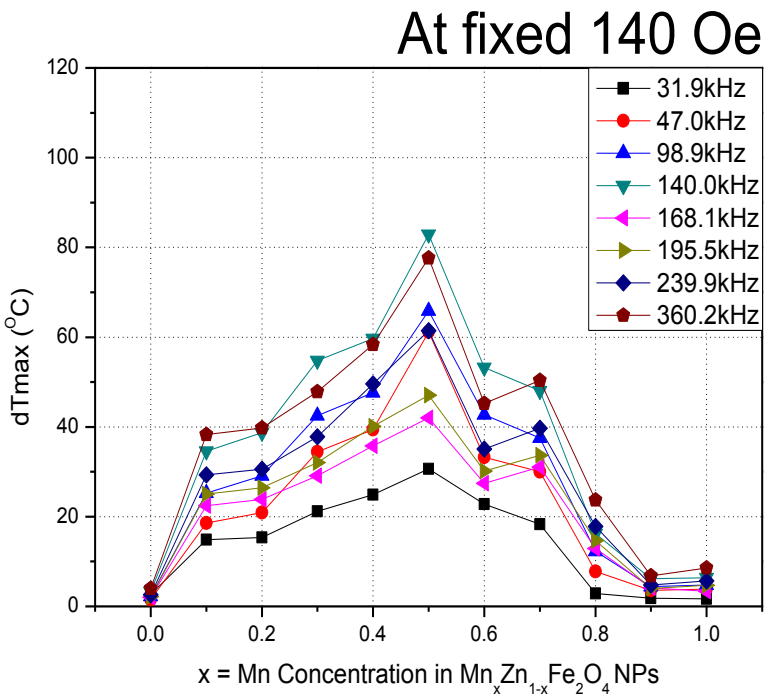

Figure 7-4. AC magnetically induced self-heating characteristics of $Mn_xZn_{1-x}Fe_2O_4$ solid state nanoparticles depending on the Mn concentration at fixed 140 Oe. (t=600 seconds)

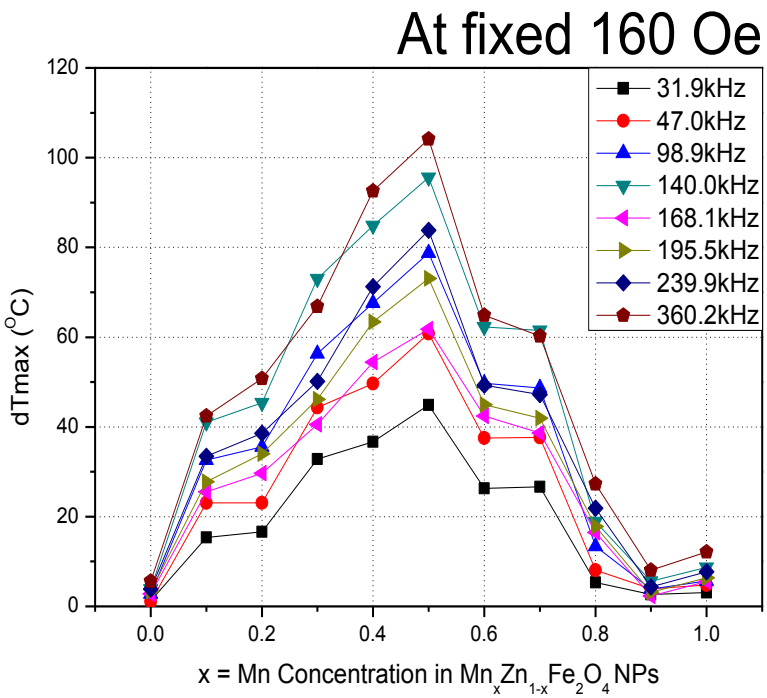

Figure 7-5. AC magnetically induced self-heating characteristics of $Mn_xZn_{1-x}Fe_2O_4$ solid state nanoparticles depending on the Mn concentration at fixed 160 Oe. (t=600 seconds)

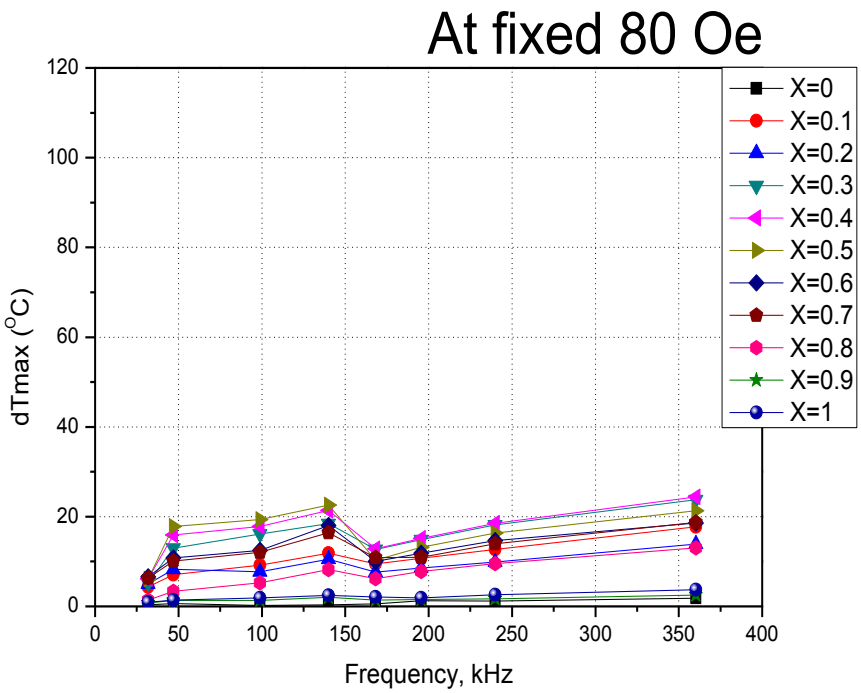

Figure 7-6. AC magnetically induced self-heating characteristics of $Mn_xZn_{1-x}Fe_2O_4$ solid state nanoparticles depending on the frequencies at fixed 80 Oe. (t=600 seconds)

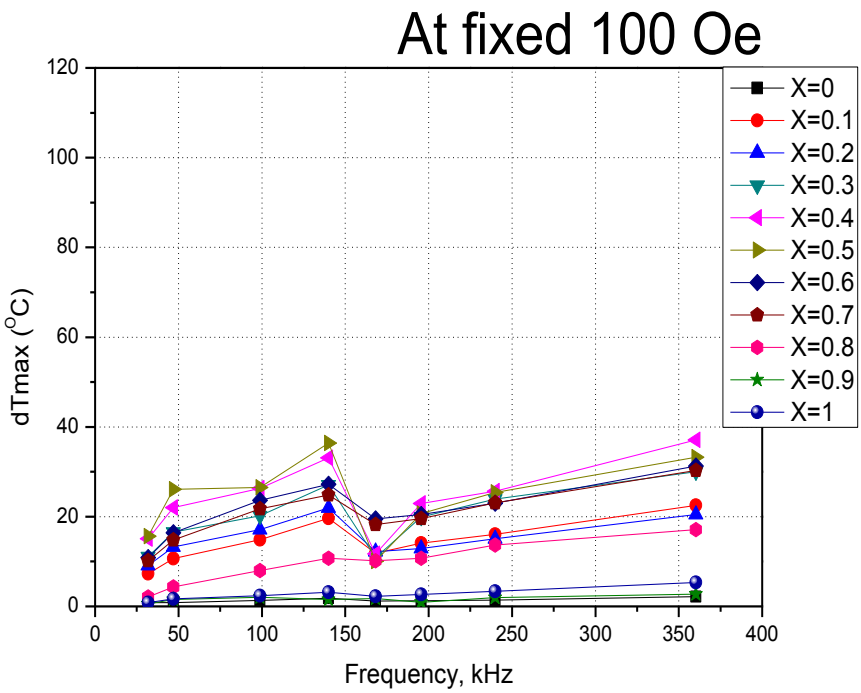

Figure 7-7. AC magnetically induced self-heating characteristics of $Mn_xZn_{1-x}Fe_2O_4$ solid state nanoparticles depending on the frequencies at fixed 100 Oe. (t=600 seconds)

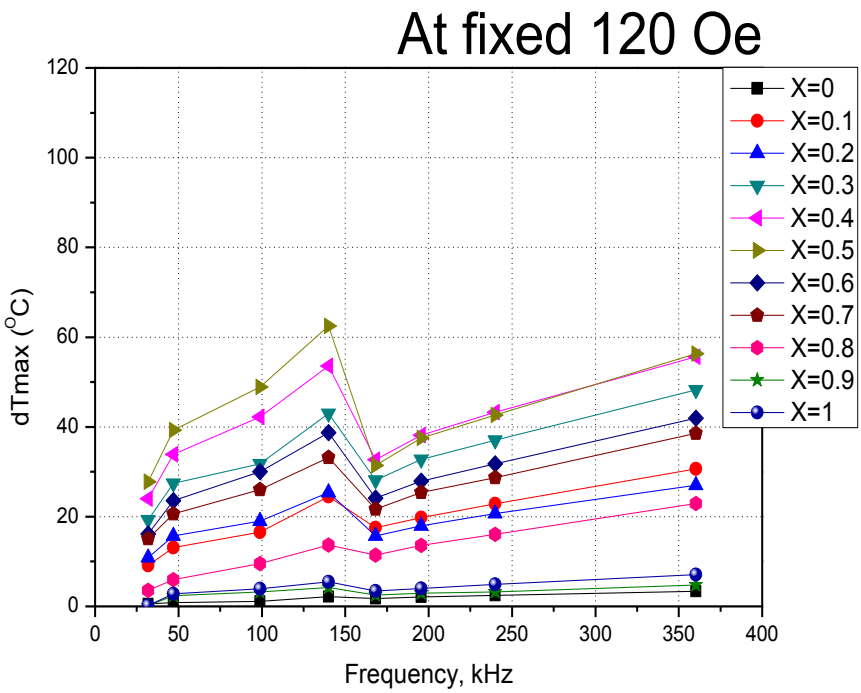

Figure 7-8. AC magnetically induced self-heating characteristics of $Mn_xZn_{1-x}Fe_2O_4$ solid state nanoparticles depending on the frequencies at fixed 120 Oe. (t=600 seconds)

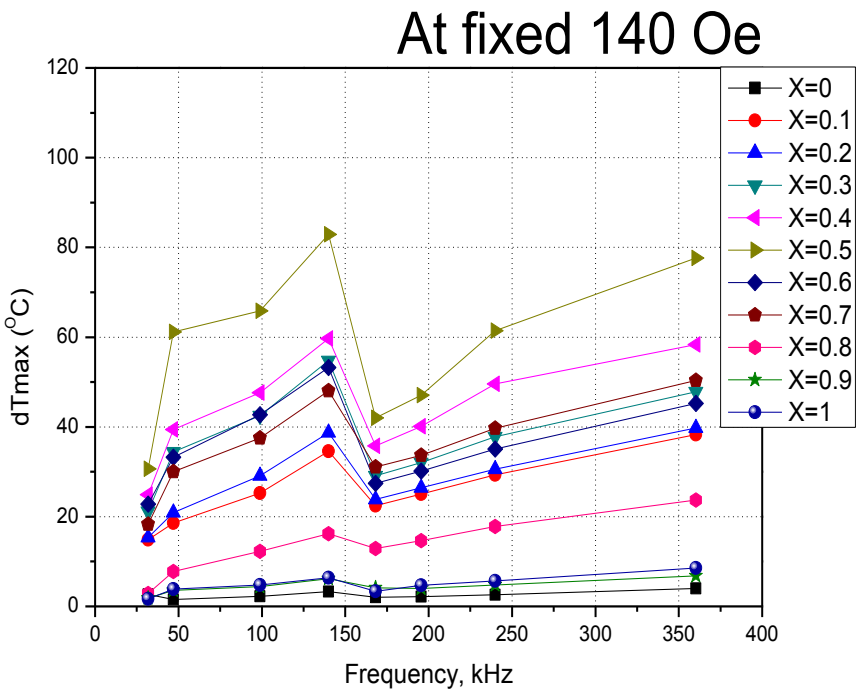

Figure 7-9. AC magnetically induced self-heating characteristics of $Mn_xZn_{1-x}Fe_2O_4$ solid state nanoparticles depending on the frequencies at fixed 140 Oe. (t=600 seconds)

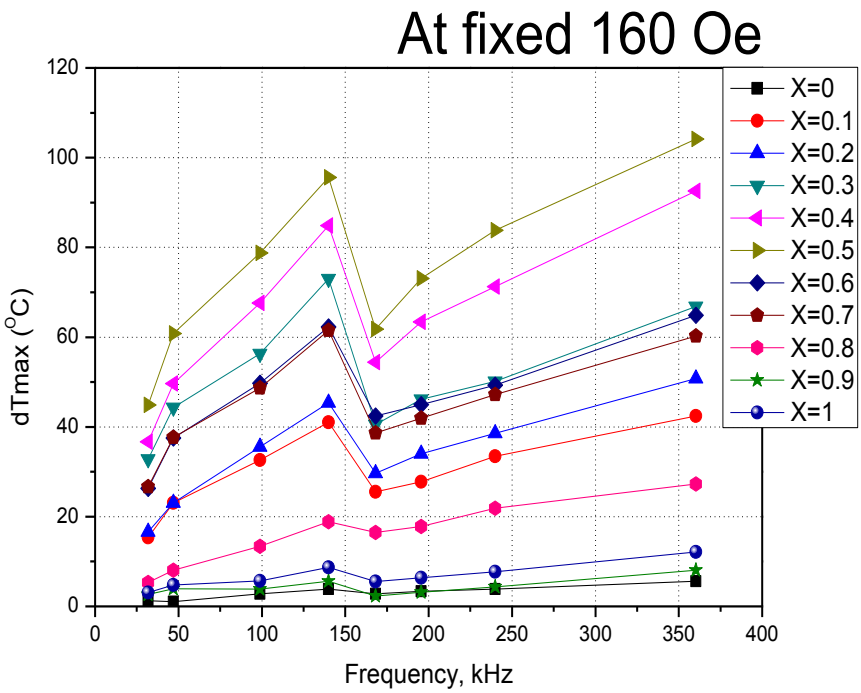

Figure 7-10. AC magnetically induced self-heating characteristics of $Mn_xZn_{1-x}Fe_2O_4$ solid state nanoparticles depending on the frequencies at fixed 160 Oe. (t=600 seconds)

At relatively low magnetic field strengths (80, 100 Oe), the maximum delta temperature value dTmax deviation of 11 kinds of $Mn_xZn_{1-x}Fe_2O_4$ nanoparticles were seem to be little in the frequencies and the doping level of manganese and zinc. However, at relatively high magnetic field strengths (120, 140, 160 Oe), $Mn_{0.5}Zn_{0.5}Fe_2O_4$ nanoparticle (X=0.5, at the middle of the X axis in figure 7-3~5) exhibits highest dTmax value, verifying that the $Mn_{0.5}Zn_{0.5}Fe_2O_4$ nanoparticles are generating highest AC heating characteristics at every frequencies. Moreover, as shown in figure 7-8~10, the dTmax value of AC heating characteristics at the frequency of 140.0 kHz and 360.2 kHz were relatively high, implying that the nanoparticles used in this study responses with the extremely low frequencies compare to the other groups. [7, 8, 9] This result takes great advantage because when it comes to say magnetic nanoparticle hyperthermia or magnetic nanofluid hyperthermia on *in vivo* models or clinical approaches, the following AC magnetic field and frequency is strictly restricted. To establish magnetic nanoparticle hyperthermia on

animal experimental models or humans, the applied magnetic field strength must be lower than 190 Oe, and the applied frequency must below 100 kHz as called as "biologically and physiologically safe range". [10] The superparamagnetic $Mn_{0.5}Zn_{0.5}Fe_2O_4$ nanoparticle, as shown in figure 7, exhibits highest AC heating characteristics and also generates relatively high AC heating characteristics on 98.9 kHz, implying that the superparamagnetic $Mn_{0.5}Zn_{0.5}Fe_2O_4$ nanoparticle has a potentiality for clinical magnetic nanoparticle hyperthermia application.

in vitro cytotoxicity assay of PEGylated $Mn_{0.5}Zn_{0.5}Fe_2O_4$ nanoparticles

For the application of $Mn_{0.5}Zn_{0.5}Fe_2O_4$ magnetic nanoparticle hyperthermia *in vitro*, cytotoxicity assay were done with 11 different kinds of human derived cells, concretely 7 kinds of commercially available human glioblastoma cell lines (A172, T98G, U87, U118, U138, U251, U373), primary cultured human glioblastoma cells (GBL-28 and GBL-37), and primary cultured human normal cortex cells (NSC10, NSC09). Within the

100 μg/ml of nanoparticle concentration, the relative cell viability of 11 kinds of the cells exceeded 70 %, indicating that the nanoparticle itself is not critically influenced the cell viability, and is also stable when the nanoparticles are incubated with the cells.

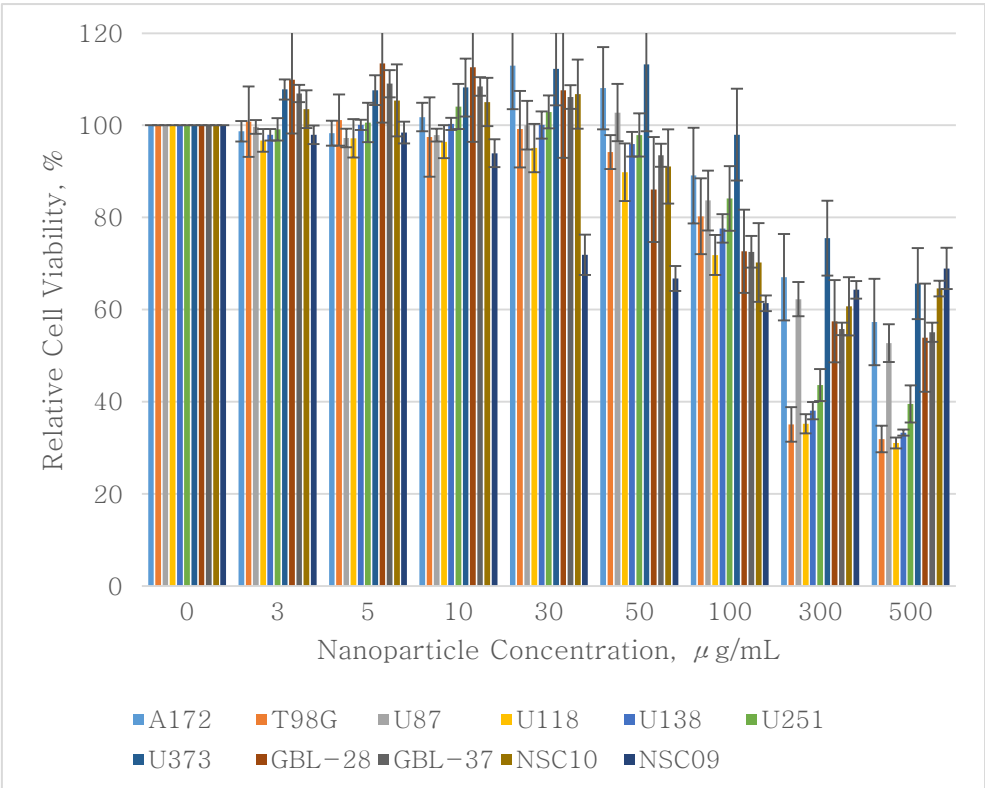

Figure 8. *in vitro* cytotoxicity (cell viability) assay of PEGylated $Mn_{0.5}Zn_{0.5}Fe_2O_4$ nanoparticles on different kinds of human glioblastoma cells and normal cortex cells.

Cellular uptake behavior of PEGylated $Mn_{0.5}Zn_{0.5}Fe_2O_4$ nanoparticles

The cellular uptake behavior of PEGylated $Mn_{0.5}Zn_{0.5}Fe_2O_4$ nanoparticles by the 11 kinds of human derived cells and its morphological change caused by the PEGylated $Mn_{0.5}Zn_{0.5}Fe_2O_4$ nanoparticles were investigated by the TEM with the concentration of 100 μg/mL of nanofluid, and is shown in figure 9. To successfully establish magnetic nanoparticle hyperthermia, the uptake or absorbed nanoparticles must be localized inside the cells without side effects such as inflammations, nucleus fragmentation, or cellular deformation. As seen in figure 9, all of the absorbed nanoparticles were located in the cytoplasmic area without disturbing or affecting the nucleus or nuclear membrane. If PEGylated nanoparticles are infused in the tumoral area and exposed to the AC magnetic fields, the absorbed nanoparticles can directly destroy the cytoplasmic area or cell membrane of malignant tumor cells, also induces programmed cell death in consequence of the raised temperature during magnetic nanoparticle hyperthermia.

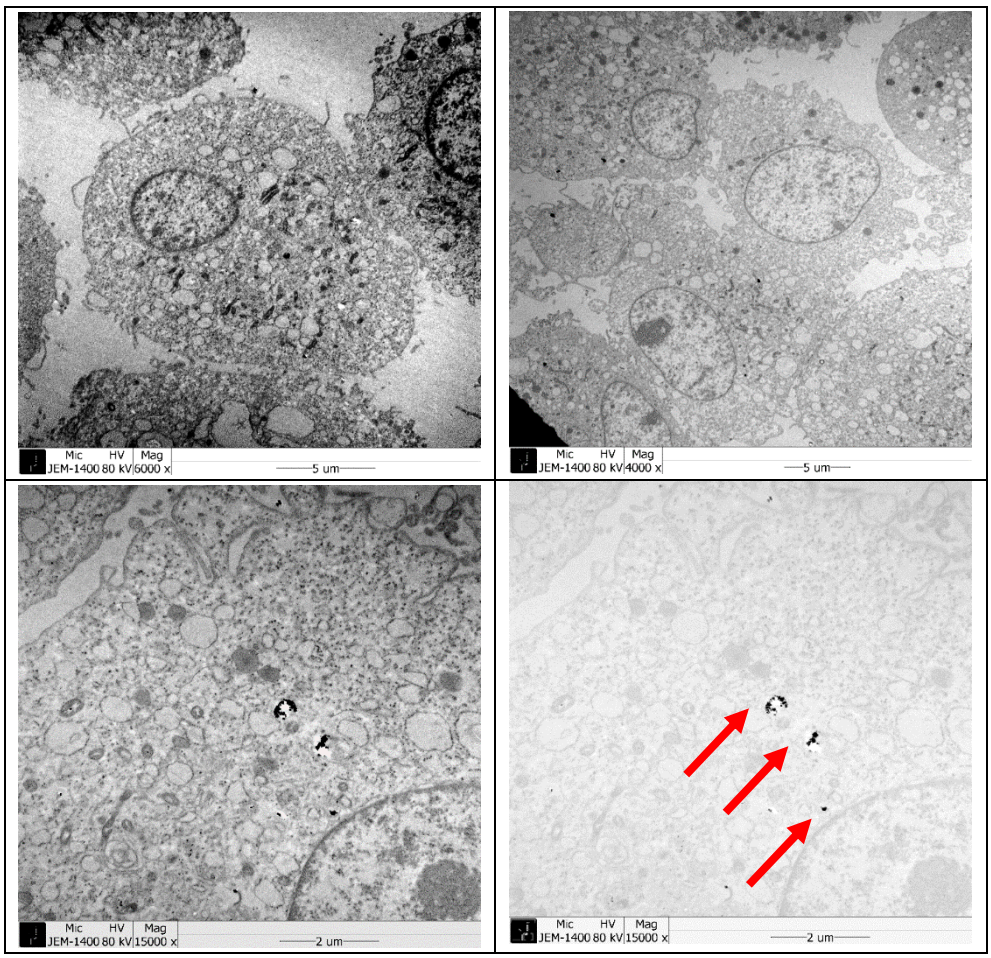

Figure 9-1. TEM images of U87 with PEGylated $Mn_{0.5}Zn_{0.5}Fe_2O_4$ nanoparticles. Contrast decreased image (bottom right) indicates that the red arrows in the picture are internalized nanoparticles.

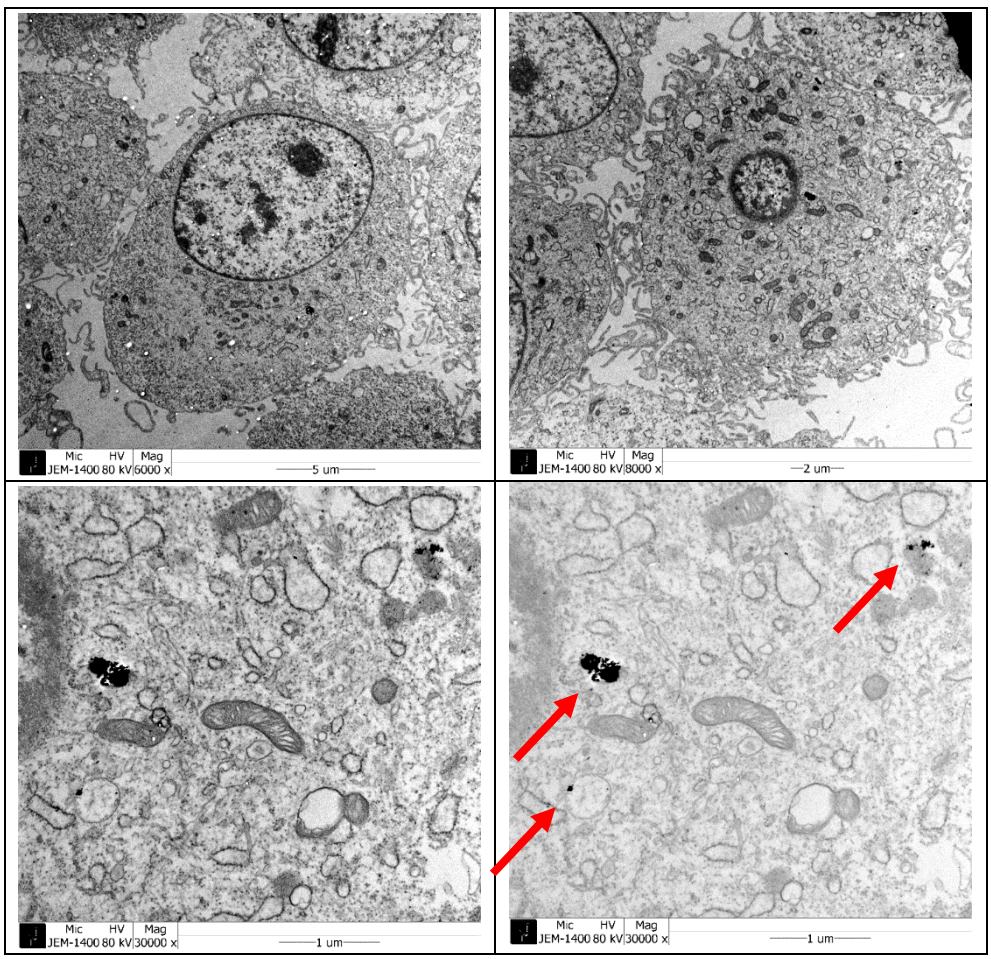

Figure 9-2. TEM images of U118 with PEGylated $Mn_{0.5}Zn_{0.5}Fe_2O_4$ nanoparticles. Contrast decreased image (bottom right) indicates that the red arrows in the picture are internalized nanoparticles.

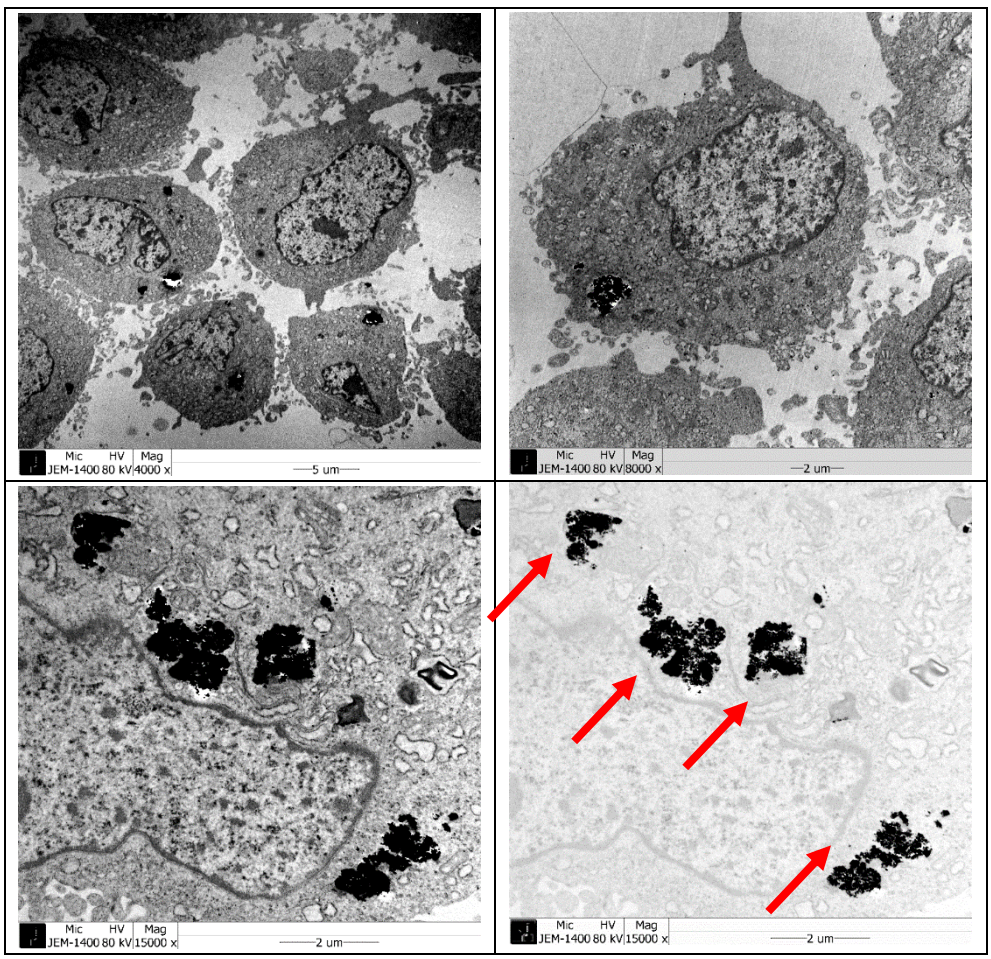

Figure 9-3. TEM images of U138 with PEGylated $Mn_{0.5}Zn_{0.5}Fe_2O_4$ nanoparticles. Contrast decreased image (bottom right) indicates that the red arrows in the picture are internalized nanoparticles.

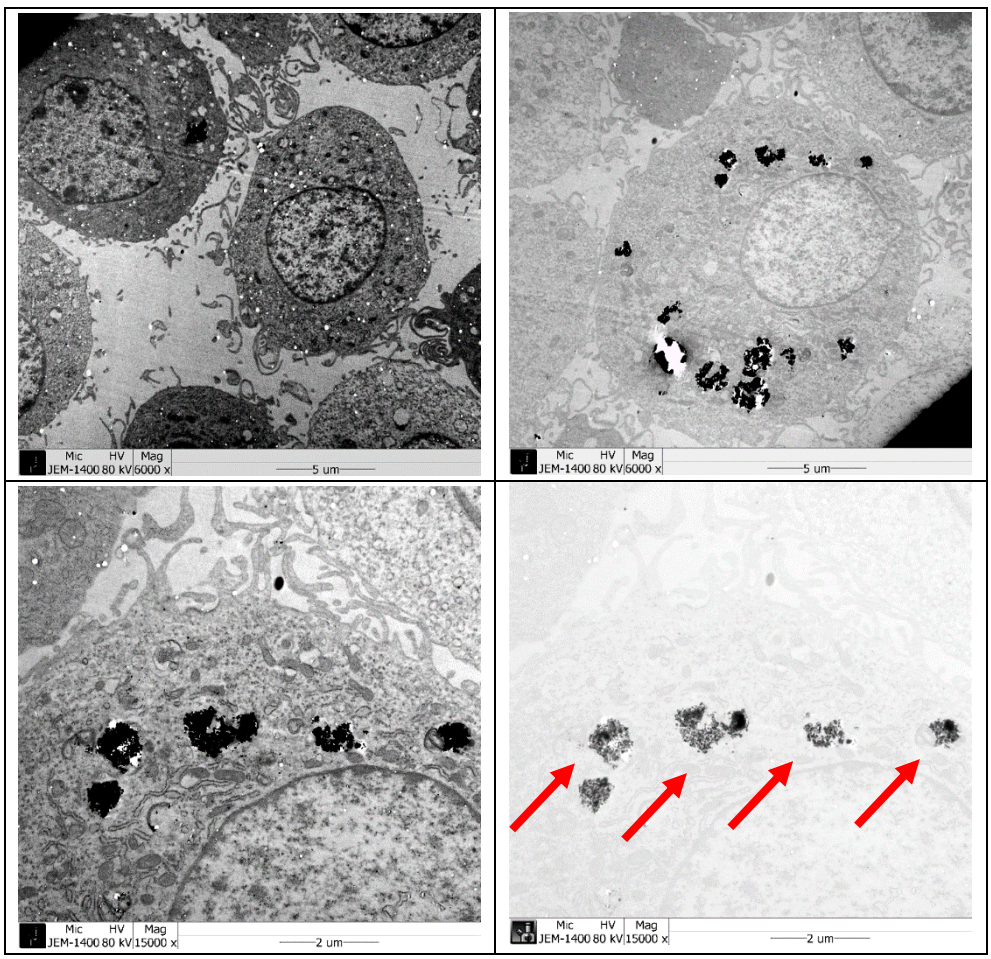

Figure 9-4. TEM images of U251 with PEGylated $Mn_{0.5}Zn_{0.5}Fe_2O_4$ nanoparticles. Contrast decreased image (bottom right) indicates that the red arrows in the picture are internalized nanoparticles.

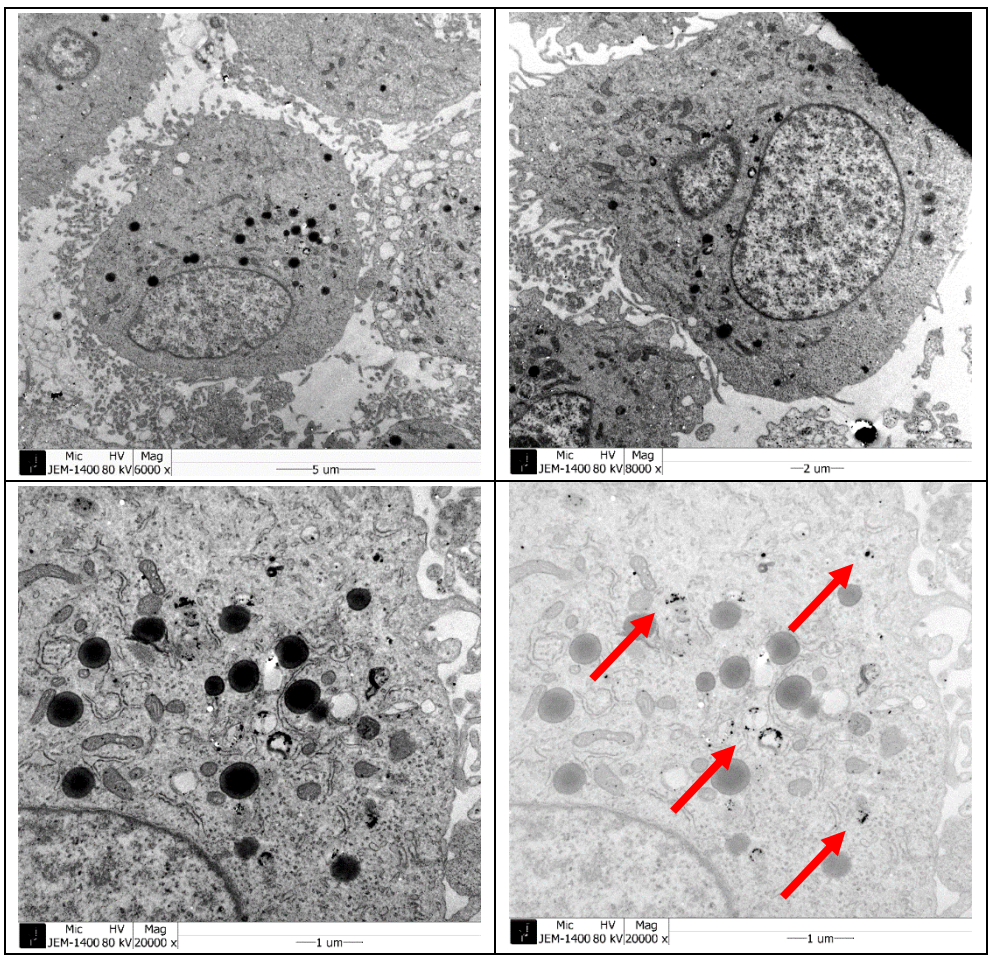

Figure 9-5. TEM images of U373 with PEGylated $Mn_{0.5}Zn_{0.5}Fe_2O_4$ nanoparticles. Contrast decreased image (bottom right) indicates that the red arrows in the picture are internalized nanoparticles.

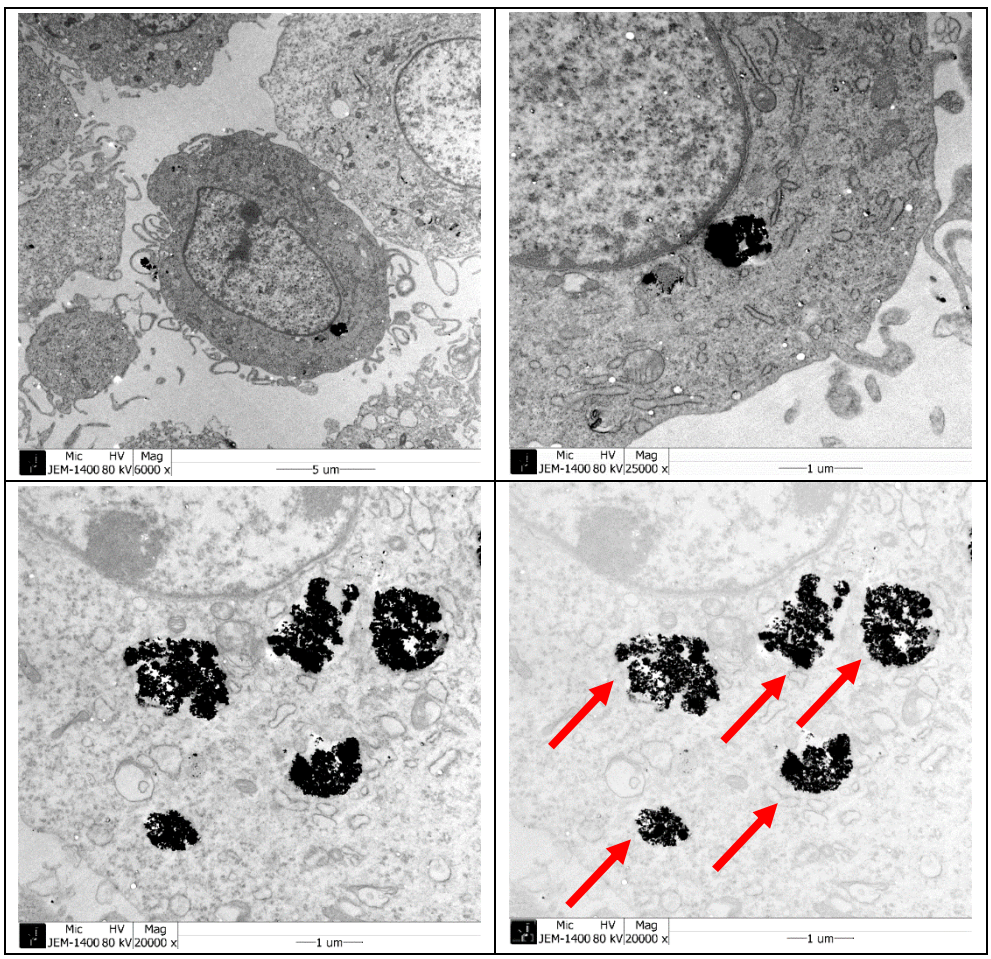

Figure 9-6. TEM images of T98G with PEGylated $Mn_{0.5}Zn_{0.5}Fe_2O_4$ nanoparticles. Contrast decreased image (bottom right) indicates that the red arrows in the picture are internalized nanoparticles.

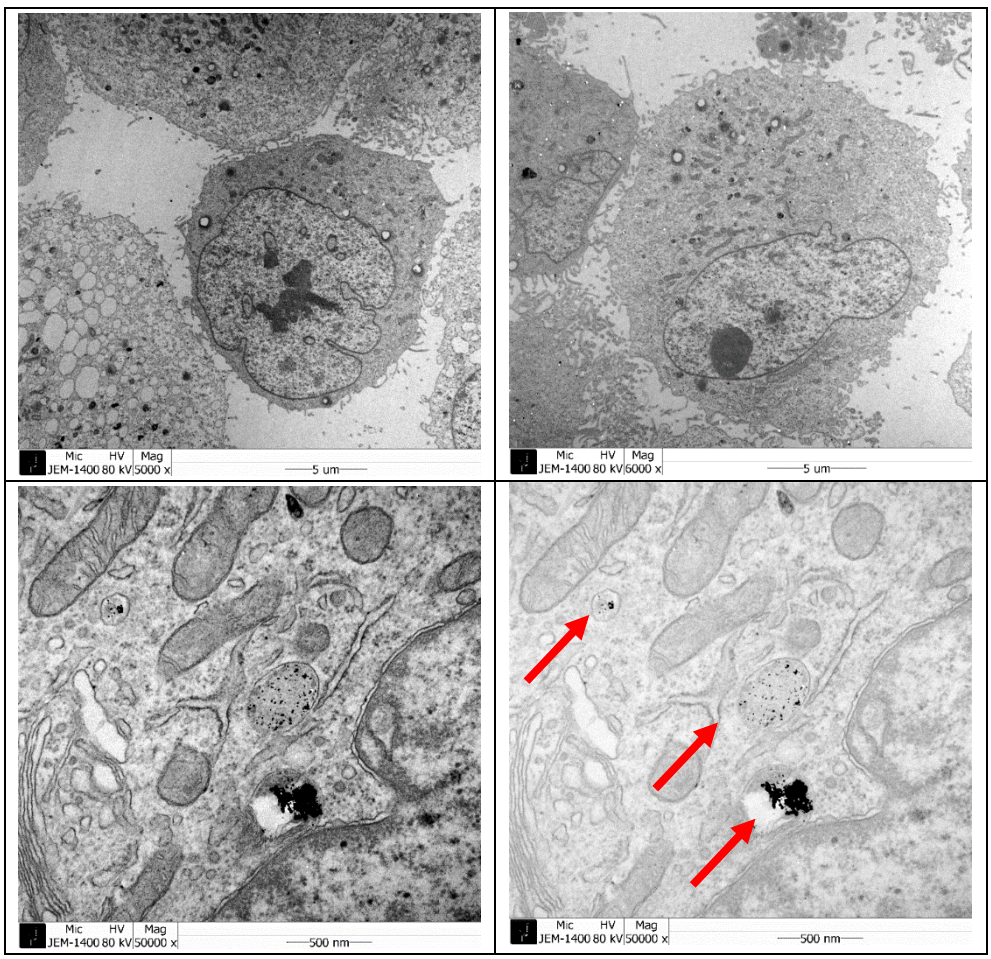

Figure 9-7. TEM images of A172 with PEGylated $Mn_{0.5}Zn_{0.5}Fe_2O_4$ nanoparticles. Contrast decreased image (bottom right) indicates that the red arrows in the picture are internalized nanoparticles.

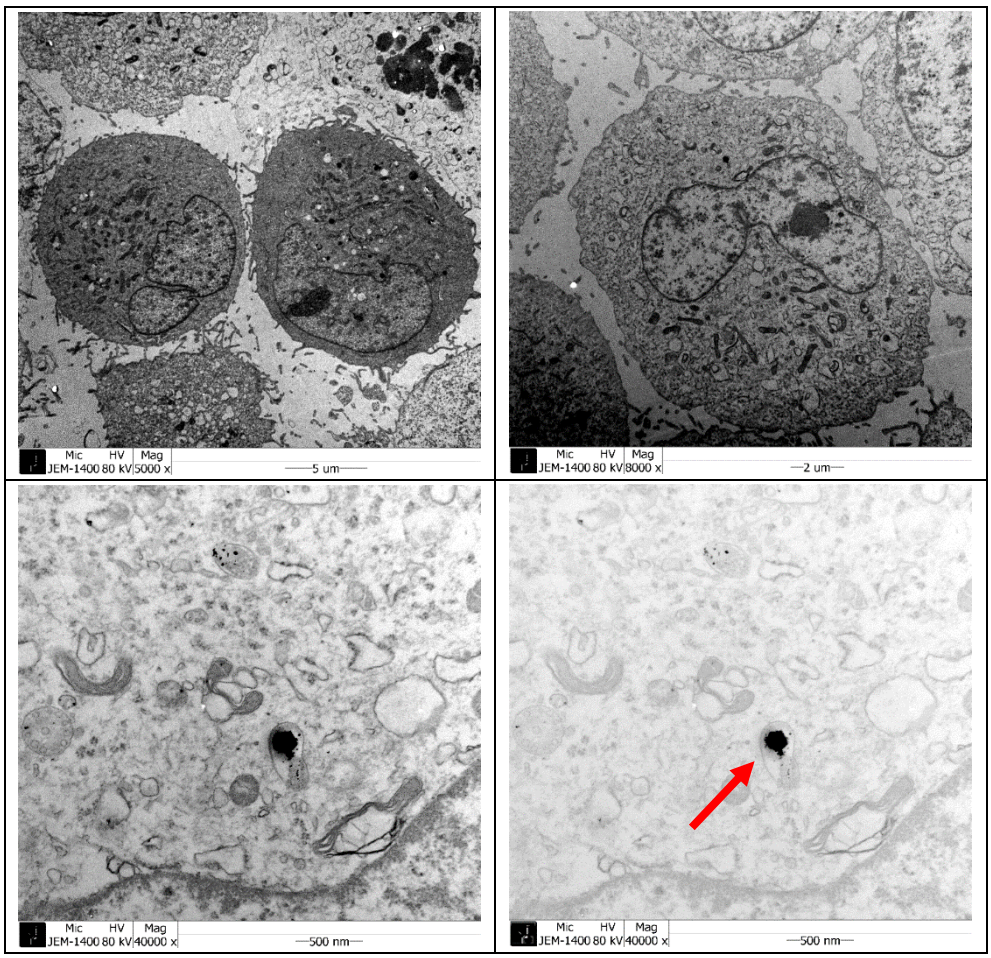

Figure 9-8. TEM images of GBL-28 with PEGylated $Mn_{0.5}Zn_{0.5}Fe_2O_4$ nanoparticles. Contrast decreased image (bottom right) indicates that the red arrows in the picture are internalized nanoparticles.

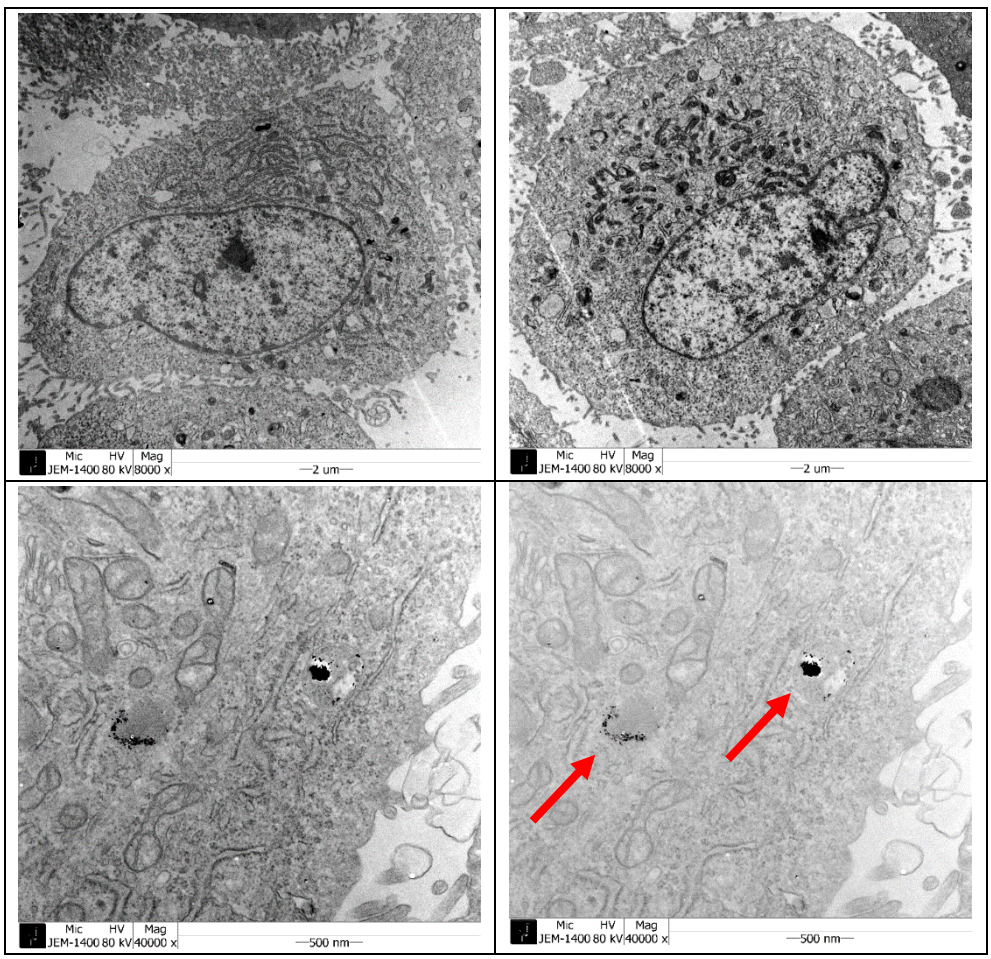

Figure 9-9. TEM images of GBL-37 with PEGylated $Mn_{0.5}Zn_{0.5}Fe_2O_4$ nanoparticles. Contrast decreased image (bottom right) indicates that the red arrows in the picture are internalized nanoparticles.

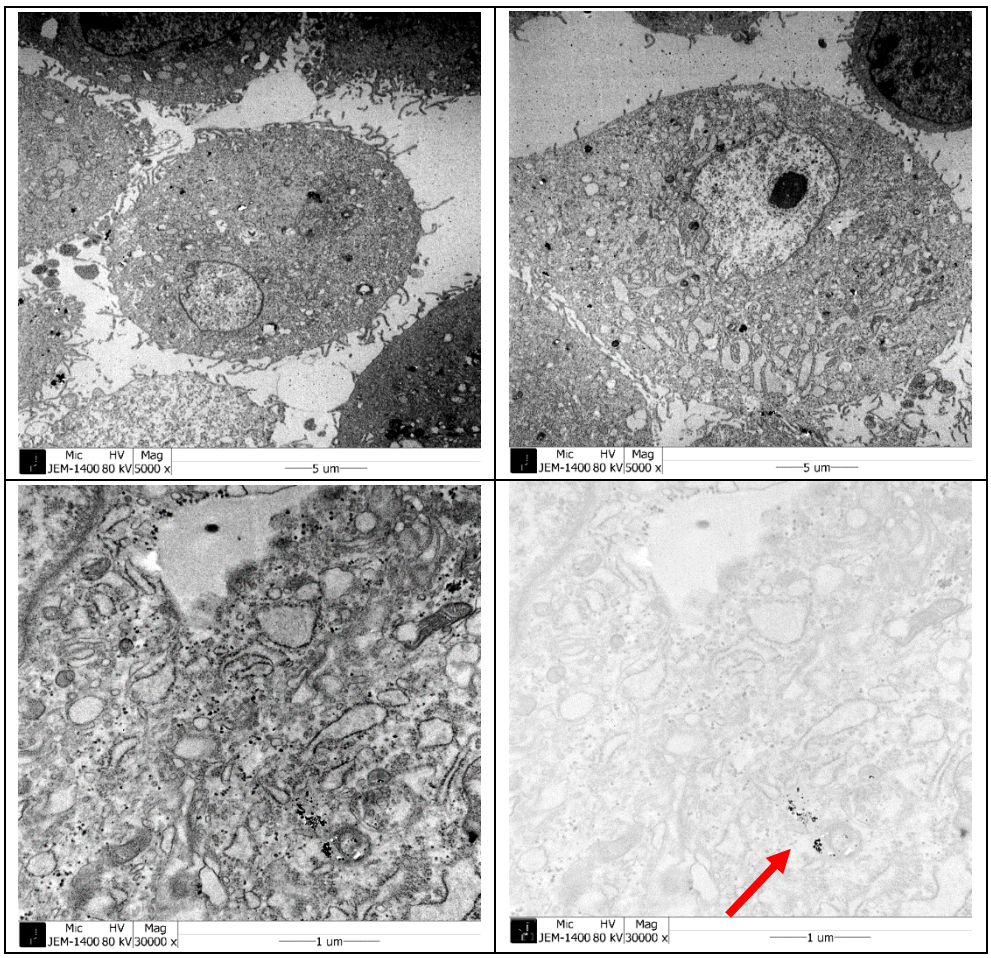

Figure 9-10. TEM images of NSC10 with PEGylated $Mn_{0.5}Zn_{0.5}Fe_2O_4$ nanoparticles. Contrast decreased image (bottom right) indicates that the red arrows in the picture are internalized nanoparticles.

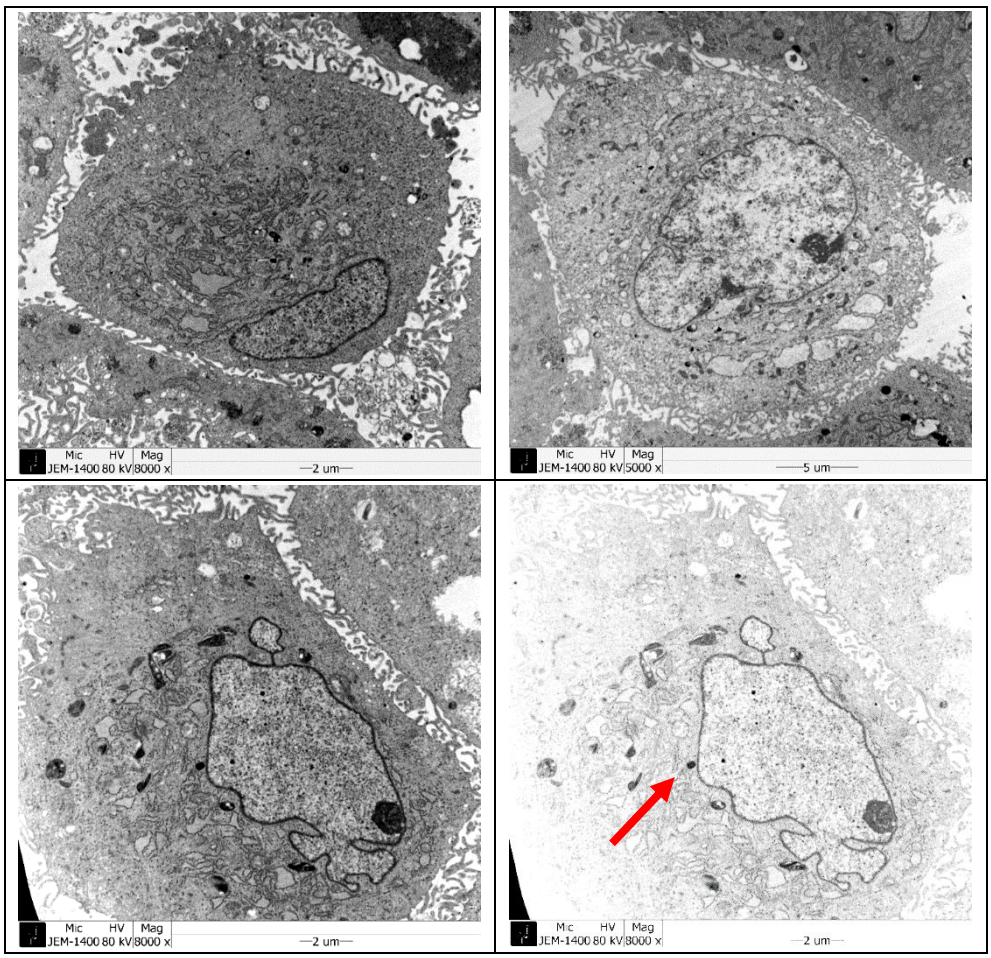

Figure 9-11. TEM images of NSC09 with PEGylated $Mn_{0.5}Zn_{0.5}Fe_2O_4$ nanoparticles. Contrast decreased image (bottom right) indicates that the red arrows in the picture are internalized nanoparticles.

in vivo magnetic nanoparticle hyperthermia application

To investigate the *in vivo* therapeutic efficacy of the magnetic nanoparticle hyperthermia, the PEGylated $Mn_{0.5}Zn_{0.5}Fe_2O_4$ nanofluids were injected at the center of the subcutaneous xenografted tumors induced by FSaLL cells. Mouse were exposed with AC magnetic fields, and the surface temperature during magnetic nanoparticle hyperthermia was monitored with thermal camera as shown in figure 10. The skin surface temperature of tumor exceeded 38.3 ℃ during magnetic hyperthermia, and it is also can be interpreted that the inner or core temperature of the tumor during hyperthermia can be higher than skin temperature. Moreover, the temperature difference between the tumoral area and normal body temperature were analyzed with thermal camera software called ResearchIR (FLIR, Wilsonville, USA), showing that the temperature difference of tumor and the body temperature was more than 5 ℃ as shown in figure 11.

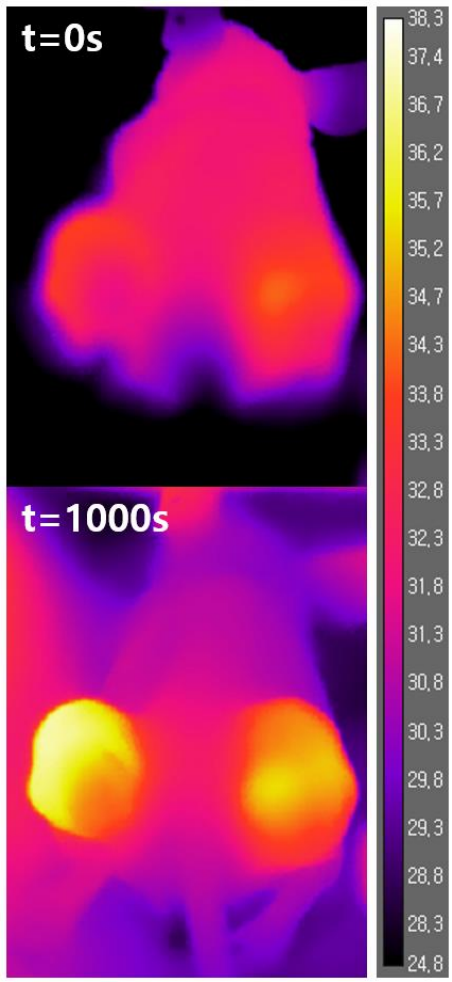

Figure 10. Thermal image of a mouse tumor model exposed to AC magnetic field for 20 minutes after injection with PEGylated $Mn_{0.5}Zn_{0.5}Fe_2O_4$ nanoparticles.

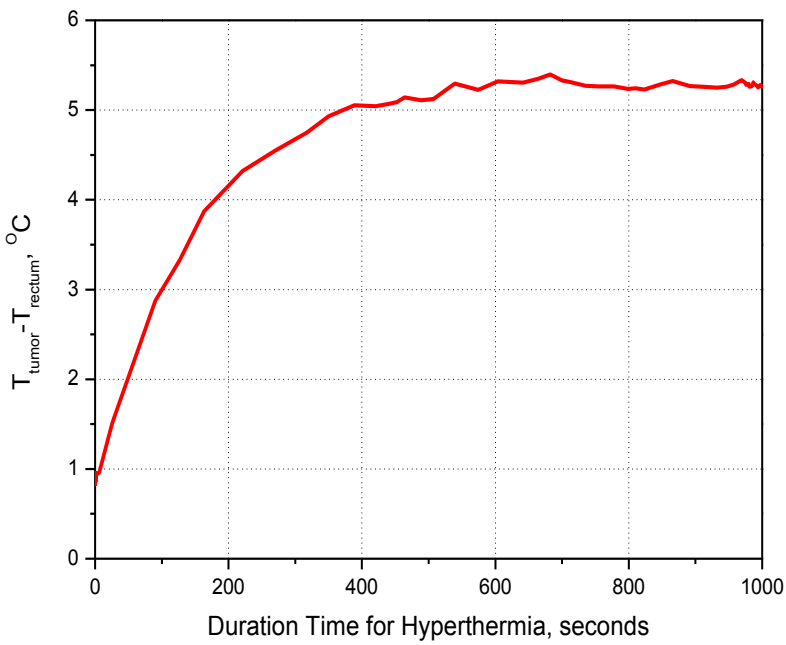

Figure 11. Relative temperature difference between tumor and body during magnetic nanoparticle hyperthermia.

After 6 minutes of AC magnetic field exposure, the hyperthermic temperature was obtained at the tumor, and the temperature was maintained during hyperthermia treatment. Also, the tumor size were measured with Vernier caliper, and the volumetric tumor size calculation was done by using tumor volume calculation formula [11]. As seen in figure 12-1, tumor size with control group and magnetic nanoparticle only were significantly increased after treatment started, with the size increased more than 15 times. However, the hyperthermia group, which is given with magnetic nanoparticle and AC magnetic field, the increase rate of the tumor size were slower than the other groups, and the tumor size were also smaller than the other groups. Thus, the hyperthermia treatment using magnetic nanoparticle can inhibit the tumor growth, but the tumor was not completely cured. Figure 12-2 shows the relative change of body weight during the treatment schedule, showing that there was no significant difference of the body weight except hyperthermia group. We assume that the difference of the body weight comes from the enlarged tumor volume.

Figure 13 shows the captured image of subcutaneous tumors during magnetic nanoparticle hyperthermia.

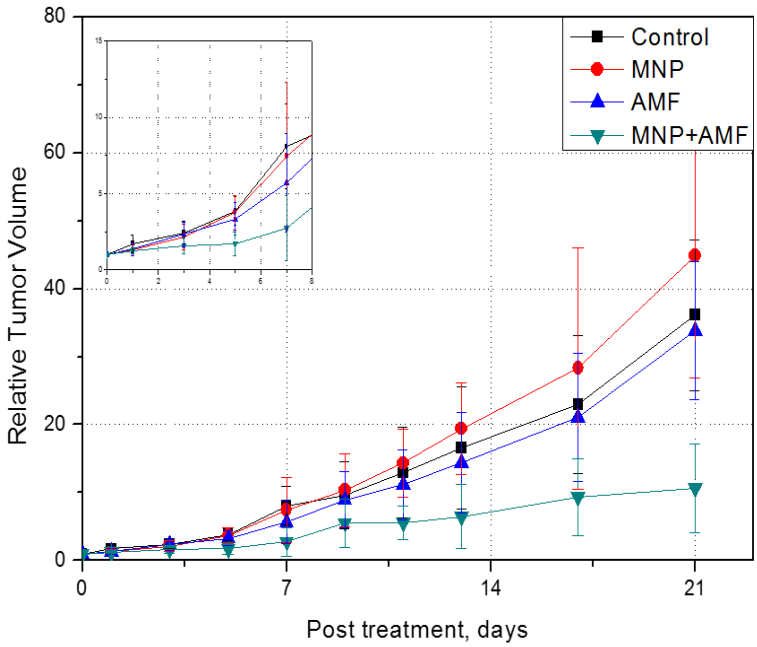

Figure 12-1. Relative tumor volume during hyperthermia treatment. Control group (black), tumors with magnetic nanoparticle only (red), tumors with magnetic field only (blue), and tumors with magnetic nanoparticle hyperthermia (green)

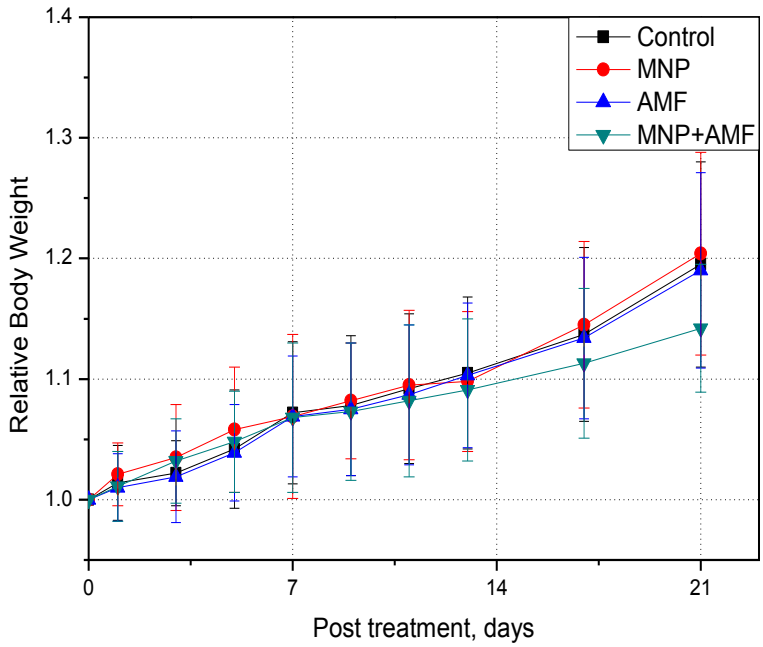

Figure 12-2. Relative body weight during hyperthermia treatment. Control group (black), tumors with magnetic nanoparticle only (red), tumors with magnetic field only (blue), and tumors with magnetic nanoparticle hyperthermia (green)

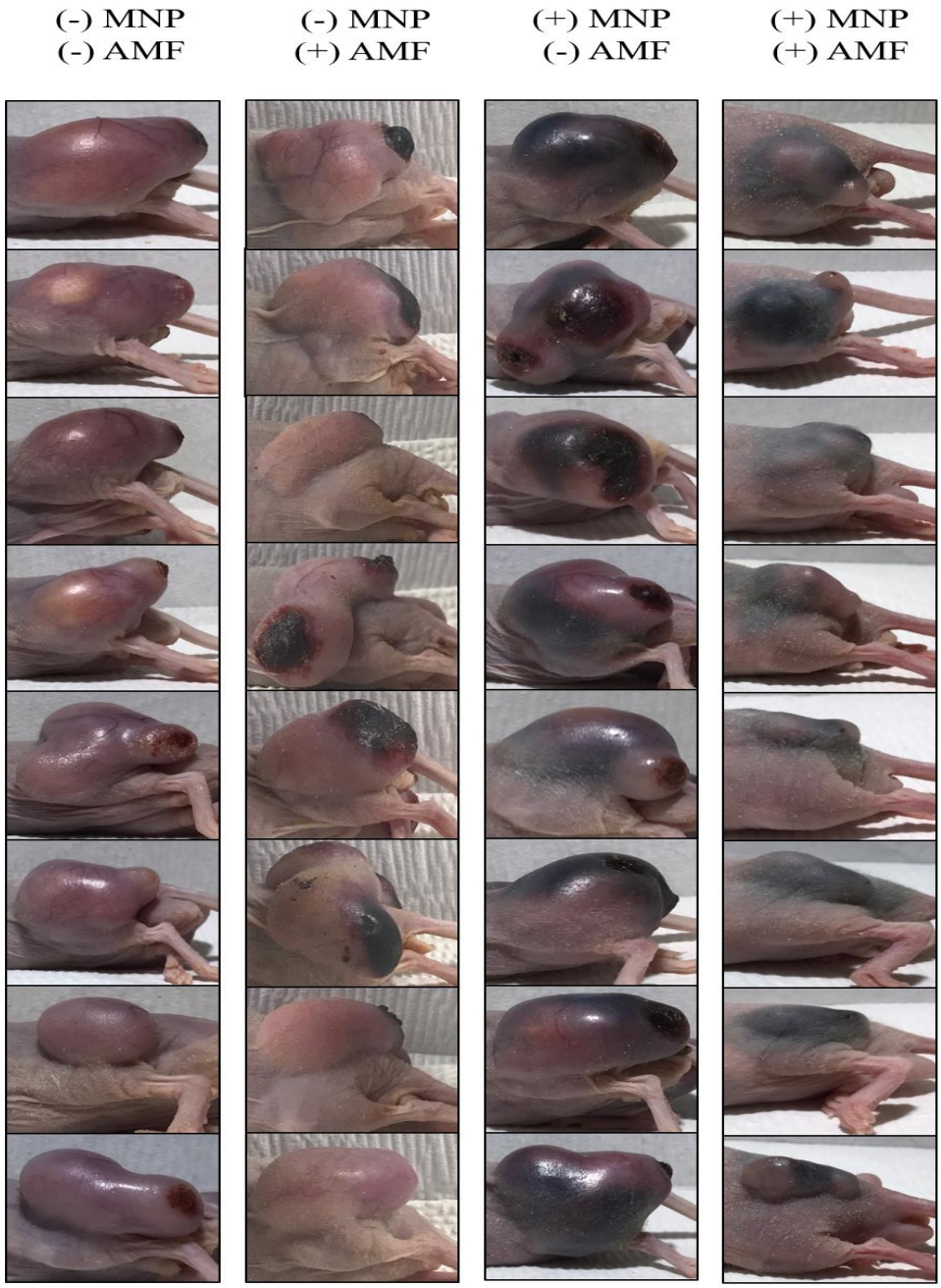

Figure 13. Image of subcutaneous tumors after hyperthermia treatment.

Besides, magnetic nanoparticle hyperthermia application has a lot of advantages compared with conventional heat treatment such as ultrasound, focused ultrasound, microwave, radio frequency probe hyperthermia, and radio frequency capacitance hyperthermia. [12] For example, ultrasound and focused ultrasound can deeply penetrate to the organs, but it can influence the bone with high energy absorption and immoderate reflection from the surrounding air. Heat treatment as microwave has poor penetration depth, and radio frequency probe hyperthermia has disadvantage such as insufficient accessibility to the deeply located tumors. However, magnetic nanoparticle hyperthermia has several kinds of advantages compared with conventional heat treatment methods. First, magnetic nanoparticle hyperthermia can treat deep seated tumors. With using intratumoral nanoparticle injection method, the heat induced from injected nanoparticle and external magnetic field can treat deeply located tumors such as brain tumors. Second, magnetic nanoparticle hyperthermia can generate high temperature selectively and uniformly, because the

dispersed magnetic nanoparticle located at the target organ can continuously reacts with external magnetic fields when it is applied. To conclude, because the given external magnetic fields can only reacts with magnetic compounds, the adjoining organs consists of healthy tissues are not influenced with the magnetic fields. The major limitation of radio frequency probe and capacitance hyperthermia is that the generated electric field can penetrate the surrounding healthy tissue that result in unwanted heating of the particular region, but magnetic nanoparticle hyperthermia can selectively focus the tumors and continuously generate the heating temperature, without affecting the surrounding healthy tissues.

CONCLUSION

In this study, the $Mn_xZn_{1-x}Fe_2O_4$ nanoparticles were successfully synthesized with controlled doping level of manganese and zinc. Their nanoparticle size and size distribution were investigated via TEM analysis, showing that the 11 kinds of $Mn_xZn_{1-x}Fe_2O_4$ nanoparticles were synthesized well within the size of below 10 nanometers. The AC heating characteristics were measured with specially designed AC magnetic field generation system, exhibiting that the $Mn_{0.5}Zn_{0.5}Fe_2O_4$ nanoparticles can generate highest AC heating temperature in several kinds of frequencies. Moreover, surface modification of $Mn_{0.5}Zn_{0.5}Fe_2O_4$ nanoparticles were done with methoxy-PEG-silane, to give functionality for $Mn_{0.5}Zn_{0.5}Fe_2O_4$ nanoparticles so that the magnetic nanofluid can be used for *in vitro* and *in vivo* biocompatibility study. However, to consider the biologically and physiologically safe range of magnetic field, we fixed the frequency with 99.0 kHz and the magnetic field with 140 Oe. *in vivo* magnetic nanoparticle

hyperthermia study was done with subcutaneous mouse tumor models, indicating that the magnetic hyperthermia can help to resist the tumor growth and tumor survival. However, magnetic nanoparticle hyperthermia therapy cannot completely cured the tumor, but the hyperthermia treatment inhibited the tumor growth rate. To accomplish successful preclinical or clinical hyperthermia treatment, the suitable AC magnetic field administration time and magnetic nanofluid concentration must be investigated. Moreover, adequate hyperthermic temperature should be generated under biologically and physiologically safe range of magnetic field strength, so that the elevated temperature can reduce the tumor size or help the therapeutic efficacy of conventional therapy such as chemotherapy or radiation therapy.

REFERENCES

[1] Jon Dobson, Magnetic Nanoparticles for Drug Delivery, DRUG DEVELOPMENT RESEARCH, 67, 55~60 (2006)

[2] An-Hui Lu, E. L. Salabas, Ferdi Schuth, Magnetic Nanoparticles: Synthesis, Protection, Functionalization, and Application, ANGEWANTE CHEMIE, 46, 1222~1244 (2007)

[3] Georgia C. Papaefthymiou, Nanoparticle magnetism, NANO TODAY, 4, 438~447 (2009)

[4] Q A Pankhurst, J Connolly, S K Jones, J Dobson, Applications of magnetic nanoparticles in biomedicine, JOURNAL OF PHYSICS D: APPLIED PHYSICS, 36, R167~R181 (2003)

[5] Wei Rao, Zhong-Shan Deng, Jing Liu, a Review of Hyperthermia Combined With Radiotherapy/Chemotherapy on Malignant Tumors, CRITICAL REVIEWS IN BIOMEDICAL ENGINEERING, 38(1), 101~116 (2010)

[6] Shouheng Sun, Hao Zeng, David B. Robinson, Simone Raoux, Philip M. Rice, Shan X. Wang and Guanxiong Li, Monodisperse MFe2O4 (M = Fe, Co, Mn) Nanoparticles, JOURNAL OF THE AMERICAN CHEMICAL SOCIETY, 126(1), 273~279 (2004)

[7] Hui S Huang, James F Hainfeld, Intravenous magnetic nanoparticle cancer hyperthermia, INTERNATIONAL JOURNAL OF NANOMEDICINE, 8, 2521~2532 (2013)

[8] Susanne Kossatz, Robert Ludwig, Heidi Dahring, Volker Ettelt, Gabriella Rimkus, Marzia Marciello, Gorka Salas, Vijay Patel, Francisco J.

Teran, Ingrid Hilger, High Therapeutic Efficiency of Magnetic Hyperthermia in Xenograft Models Achieved with Moderate Temperature Dosages in the Tumor Area, PHARMACEUTICAL RESEARCH, 31, 3274~3288 (2014)

[9] Kun Fang, Lina Song, Zhuxiao Gu, Fang Yang, Yu Zhang, Ning Gu, Magnetic field activated drug release system based on magnetic PLGA microspheres for chemo-thermal therapy, COLLOIDS AND SURFACES B: BIOINTERFACES, 136, 712~720 (2015)

[10] Andreas Jordan, Regina Scholz, Peter Wust, Horst Fahling, Roland Felix, Magnetic fluid hyperthermia (MFH): Cancer treatment with AC magnetic field induced excitation of biocompatible superparamagnetic nanoparticles, JOURNAL OF MAGNETISM AND MAGNETIC MATERIALS, 201, 413~419 (1999)

[11] Monga, Satdarshan P. S. M.D.; Wadleigh, Robert M. D.; Sharma, A. M.D.; Adib, Houtan M.D.; Strader, Doris M.D.; Singh, Gurinder M.D.; Harmon, John W. M.D., Berlin, Marlene R.N.; Monga, Dulabh K. M.D.; Mishra, Lopa M.D., Intratumoral Therapy of Cisplatin/Epinephrine Injectable Gel for Palliation in Patients With Obstructive Esophageal Cancer, AMERICAN JOURNAL OF CLINICAL ONCOLOGY, 23, 4, 386~392 (2000)

[12] T. Onur Tasci, Ibrahim Vargel, Anil Arat, Elif Guzel, Petek Korkusuz, Ergin Atalar, Focused RF hyperthermia using magnetic fluids, MEDICAL PHYSICS, 36, 5, 1906~1912 (2009)

[13] Minhong Jeun, Jin Wook Jeoung, Seungje Moon, Yu Jeong Kim, Sanghoon Lee, Sun Ha Paek, Kyung-Won Chung, Ki Ho Park, Seongtae Bae, Engineered superparamagnetic Mn0.5Zn0.5Fe2O4 nanoparticles as a heat shock protein induction agent for ocular neuroprotection in glaucoma, BIOMATERIALS, 32, 387~394 (2011)

국문 초록

초상자성 산화철 나노입자의 개발과 고온열 치료의 유효성 평가

서울대학교 대학원

의학과 협동과정 종양생물학 전공

이 주 영

자성 나노 입자를 이용한 고온열 치료의 연구는 지난 수십 년간 활발하게 연구되어 오고 있다. 자성 나노 입자의 종류에는 수 나노미터의 크기를 갖는 초상자성 나노 입자부터, 수 마이크로미터의 크기를 갖는 자성 나노 로드까지 그 종류가 다양하게 보고되고 있으며, 입자 표면 개질에 사용된 고분자의 종류와 방법 또한 다양하게 보고되고 있다.

자성 나노 입자는 교류 자기장에 노출되었을 시에 자기 유도 발열 특성을 가지게 되며, 원하는 부위에 특이적으로 노출된 고열 효과는 다양한 종양 치료에 응용될 수 있다. 최근에는 고온열 치료와 화학적 항암 요법, 방사선

항암 요법을 조합한 새로운 형태의 치료 방법이 각광받고 있다.

그러나, 자성 나노 입자를 이용한 고온열 치료를 체내에 적용하기 위해서는 고려해야 할 여러 가지 요소들이 있다. 그 중에서 가장 중요한 것은 체내에 인가되는 교류 자기장의 세기와 주파수의 총량이다. 보고에 의하면 주파수와 자기장 세기의 총량이 3.0×10^9 A/m•s 보다 낮은 범위에서 체내 안전하다고 알려져 있다. 이 범위 내에서 자성 나노 입자는 치료 효과를 갖는 범위 내의 온도를 유발할 수 있어야 하며, 주변의 정상 조직과 장기에 영향을 미치지 않아야 한다. 이와 같은 관점에서, 생물학적 또는 생리학적으로 안전한 범위의 자기장 내에서 충분한 자기 유도 발열 특성을 가지는 자성 나노 입자의 개발이 중요하다고 할 수 있다.

본 연구는 망간과 아연이 도핑 된 초상자성 산화 철 나노 입자의 합성과, 입자의 표면 개질, *in vitro* 생체적합성 평가와 동물 모델에서의 고온열 치료 효과 확인을 위한 실험을 포함하고 있다. 서로 다른 조성을 가지는 총 11 종류의 초상자성 산화 철 나노 입자를 합성하였고, 서로 다른 8 가지의 주파수 (31.9, 47.0, 98.9, 140.0, 168.1, 195.5, 239.9, 360.2 kHz) 와 서로 다른 5 가지의 자기장 세기 (80, 100, 120, 140, 160 Oe) 내에서 각각의 나노 입자가

가지는 자기 유도 발열 특성을 분석하였다. 또한, 자기 유도 발열 특성이 가장 높은 $Mn_{0.5}Zn_{0.5}Fe_2O_4$ 나노 입자를 methoxy-PEG-silane 으로 표면 개질하여 생체에 적합하도록 고안하였으며 세포 수준에서 나노 입자가 가지는 세포 독성 검사를 시행하였다. 여러 종류의 생체적합성 평가 실험을 거쳐 동물 종양 모델에서 자성 나노 입자를 이용한 고온열 치료의 유효성 평가에 대한 실험을 시행하였다.